Photocopy and Use Authorization

In presenting this thesis in partial fulfillment of the requirements for an advanced degree at Idaho State University, I agree that the Library shall make it freely available for inspection. I further state that permission for extensive copying of my thesis for scholarly purposes may be granted by the Dean of the Graduate School, Dean of my academic division, or by the University Librarian. It is understood that any copying or publication of this thesis for financial gain shall not be allowed without my written permission.

Signature ___________________________________

Date _______________________________________

Determining the Photon and Neutron

Flux Distributions of an Electron based Photo-Neutron Converter

By

Joe Petty

A thesis

submitted in partial fulfillment

of the requirements for the degree of

Master of Science in the Department of Physics

Idaho State University

Spring 2022

To the Graduate Faculty:

The members of the committee appointed to examine the thesis of Joe Petty find it satisfactory and recommend that it be accepted.

Dr. Tony A. Forest,
Major Advisor

Dr. Daniel S. Dale,
Committee Member

Dr. David J. Delehanty,
Graduate Faculty Representative

To My Family

Acknowledgments

I would like to thank Dr. Paul Stonaha for the opportunity to conduct this experiment at the Idaho Accelerator Center, as well as for his mentorship in using MCNP to simulate high energy particle experiments. I also thank Dr. Tony Forest for his mentorship in data and error analysis while completing this thesis. I would also like to thank Dr. Dan Dale, Justin Gahley, Sydnee Thomas, and Connor Harper for their academic assistance and support in my graduate studies. Lastly, I would like to thank Kim and Cory Petty for setting me up to succeed in college at the graduate level.

Table of Contents

List of Figures vii

List of Tables viii

Abstract x

Introduction and Theory 1 1

- Electron Linear Accelerators 1.1 2
- Bremsstrahlung Radiation 1.2 2
- Nuclear Cross Sections 1.3 3
- Radioactive Isotope Activation and Decay 1.4 4
- Photon and Neutron Activation Analysis 1.5 6
- High Purity Germanium Detectors 1.6 7
- HPGe Detector Efficiency 1.7 9
- MCNP 1.8 11

Experimental Procedure 2 14

- Photo-Neutron Converter Design 2.1 14
- Gold and Nickel Foil Placement 2.2 16
- HPGe Detector Setup 2.3 18

Data Analysis 3 21

- Multi-Channel Histogram Analysis 3.1 21
- Photon Flux Normalization 3.2 22
- Neutron Flux Normalization 3.3 28

Error Analysis 4 32

Experimental Uncertainties 4.1 32

Cross Section Uncertainties 4.2 33

Results 5 36

Bibliography 37

Appendix 39

List of Figures

Figure 1: Energy dependent cross section for 58Ni(γ,n)57Ni [1]. 3

Figure 2: HPGe data from an irradiated nickel sample. 8

Figure 3: PNC at the IAC oriented vertically. 15

Figure 4: MCNP simulated geometry of the PNC (axes in cm). 15

Figure 5: Vertical view of IAC beamline with Au1, Ni2, Au2, and Au3. 17

Figure 6: Horizontal view of IAC beamline with Au1, Ni2, and Au2. 17

Figure 7: MCNP simulated geometry of the IAC experiment. Gold foils are pink and nickel foils are green. 18

Figure 8: 14-channel fitted data for Ni2 on ROOT. 22

Figure 9: Comparison of simulated decay rate against Ni2 measurements. 24

Figure 10: Comparison of normalized decay rate against Ni2 measurements. 25

Figure 11: Photon flux distribution for nickel foils. 27

Figure 12: Photon flux distribution for gold foils. 28

Figure 13: Neutron flux distribution for nickel foils. 30

Appendix

Figure A 1: MCNP script to determine flux distributions. 46

Figure A 2: Cross section for 197Au(γ,n)196Au [2]. 76

Figure A 3: Cross section for 58Ni(n,p)58Co [4]. 77

Figure A 4: Cross section for 58Ni(γ,2n)56Ni [3]. 78

Figure A 5: Cross section for 60Ni(γ,np)58Co [5] 79

List of Tables

Table 1: List of reactions measured using PAA or NAA on the gold and nickel foils [6]. 4

Table 2: Beam time values for the IAC experiment. 14

Table 3: Foil values and geometry. 16

Table 4: HPGe specifications for the IAC detectors. 19

Table 5: List of measurements taken on Au and Ni foils. 20

Table 6: Experimental decays for 58Ni(γ,n)57Ni. 23

Table 7: Simulated decays for 58Ni(γ,n)57Ni. 23

Table 8: Experimental decays for 197Au(γ,n)196Au. 26

Table 9: Simulated decays for 197Au(γ,n)196Au. 26

Table 10: Normalization factor for photon flux. 26

Table 11: Normalized simulated decays for 58Ni(γ,n)57Ni. 27

Table 12: Normalized simulated decays for 197Au(γ,n)196Au. 27

Table 13: Experimental decays for 58Ni(n,p)58Co, 58Ni(γ,2n)56Ni, and 60Ni(γ,np)58Co........ 29

Table 14: Simulated decays for 58Ni(n,p)58Co, 58Ni(γ,2n)56Ni, and 60Ni(γ,np)58Co. 29

Table 15: Normalization factor for neutron flux. 29

Table 16: Normalized simulated decays for 58Ni(n,p)58Co, 58Ni(γ,2n)56Ni, and 60Ni(γ,np)58Co. 29

Table 17: Systematic experimental uncertainties. 33

Table 18: Summarized flux fractional uncertainties. 35

Appendix

Table A 1: Detector efficiency from the IAC. 47

Table A 2: MCNP photon flux for Ni1. 48

Table A 3: MCNP photon flux for Ni2. 50

Table A 4: Normalized photon flux for Ni1. 52

Table A 5: Normalized photon flux for Ni2. 54

Table A 6: MCNP photon flux for Au1. 56

Table A 7: MCNP photon flux for Au2. 58

Table A 8: MCNP photon flux for Au3. 60

Table A 9: Normalized photon flux for Au1. 62

Table A 10: Normalized photon flux for Au2. 64

Table A 11: Normalized photon flux for Au3. 66

Table A 12: MCNP neutron flux for Ni1. 68

Table A 13: MCNP neutron flux for Ni2. 70

Table A 14: Normalized neutron flux for Ni1. 72

Table A 15: Normalized neutron flux for Ni2. 74

Abstract

Determining the Photon and Neutron

Flux Distributions of an Electron based Photo-Neutron Converter

Thesis Abstract – Idaho State University (2022)

A photo-neutron converter (PNC) is a target used in electron linear accelerators (linac) to produce a source of neutrons that may be used for studying the neutron damage of materials. The Idaho Accelerator Center (IAC) utilizes a tungsten and zinc PNC with a 40 MeV electron beam to produce a high flux of bremsstrahlung photons and neutrons. This work measures the flux of photons and neutrons emitted from the PNC by irradiating gold and nickel foils at different angles and measuring their activity. The experiment was simulated using Monte Carlo N-Particle Transport (MCNP) to estimate the photon and neutron flux distributions. After irradiation, each of the foil's activity was measured using a high purity germanium detector. The simulated flux distributions were then normalized to match experimental results. In this experimental configuration, it was determined that there is a minimum expected neutron rate of (1.9 ± 0.4) $\times 10^{12}$ n/s from the PNC.

Key Words: PNC, Linac, IAC, MCNP

Introduction and Theory 1

A common goal in the pursuit of sustainable energy is safely increasing the operating lifetime of nuclear reactors. In order to do this, the impact of a high radiation dose on the materials used to construct nuclear reactor facilities needs to be quantified. While it is possible to examine the radiation damage over the operational life of a nuclear reactor, it is more desirable to study the effect of radiation on materials in a more controlled setting. In order to simulate the equivalent particle flux of a nuclear reactor, neutrons produced using an electron linear accelerator may be used to study an equivalent amount of radiation damage on a much shorter time scale.

A photo-neutron converter (PNC) is a target used in conjunction with electron linear accelerators to create a high flux of photons and neutrons. A PNC utilizes bremsstrahlung radiation to produce photons from the accelerated electrons. Then, the photons will produce neutrons via photo-nuclear interactions within the PNC. With a given target design, it is desirable to know the flux and energy distribution of particles coming from the PNC to determine if the neutron source can sufficiently damage materials within a short time interval. At the Idaho Accelerator Center (IAC), a tungsten and zinc PNC was designed to produce a large neutron flux and then tested using a 40 MeV linear electron accelerator. The purpose of this work is to determine the flux and energy distribution of photons and neutrons emitted at different angles by the tungsten and zinc PNC.

To accomplish this, gold (Au) and nickel (Ni) foils were irradiated at 0, 29.6, 39.5, 47.3, and 90 degree angles during the PNC experiment. Once the electron beam was turned off, the foils' activity rates were measured using techniques known as photon activation analysis (PAA) [10] and neutron activation analysis (NAA) [11]. In order to determine the shape of the flux and energy distribution, the experiment was simulated using MCNP [7]. The flux and energy distributions from MCNP were used to calculate the expected activity of the foils, and then normalized to match the experimental data. Similar experiments have been completed at the IAC by Dr. Mayir Mamtimin in his Ph.D. dissertation examining the feasibility of different PNC designs in the production of radioactive isotopes [12].

Electron Linear Accelerators 1.1

Particle accelerators are machines designed to accelerate a beam of particles to high energies and are often used to conduct particle experiments. While there are many different types of particle accelerators, this work focuses on a linear accelerator (linac) with electrons as the source particle. A linear accelerator utilizes several cavities with alternating electric fields to accelerate a charged particle down the beamline. In this experiment, the IAC's high energy S band linac was used, which is capable of accelerating electrons up to 40 MeV. The PNC was placed at the end of the beamline in order to convert the incoming electrons into photons and neutrons.

Bremsstrahlung Radiation 1.2

Bremsstrahlung radiation is responsible for the high energy photons produced by the PNC from the linac. When the electrons from the linac reach the PNC, they first scatter off of the tungsten inside the target. This rapid deceleration of electrons produces Bremsstrahlung radiation, also known as braking radiation. With any target design, it is important to note that the electron scattering rate increases as the density of the target nucleus increases. Thus, tungsten is a common material used inside PNCs due to its large atomic mass.

Nuclear Cross Sections 1.3

When an energized particle interacts with the nucleus of an atom, there is a probability of a nuclear interaction occurring. This probability is expressed as the nuclear cross section and is measured in units of cm^2 or barns (10^{-24} cm^2). An example nuclear cross section for nickel can be seen in Figure 1. In this example, an incident photon interacts with the nucleus of a Ni 58 atom, removing a neutron and converting the atom to Ni 57. It is important to note that cross sections are energy dependent, so only photons above an energy threshold have a chance of producing this reaction. The energy threshold is the binding energy of the neutron to the nucleus. In general, these cross sections are useful when it comes to measuring radioactive isotopes using photon or neutron activation analysis, and necessary when determining the particle flux incident on the materials for this work.

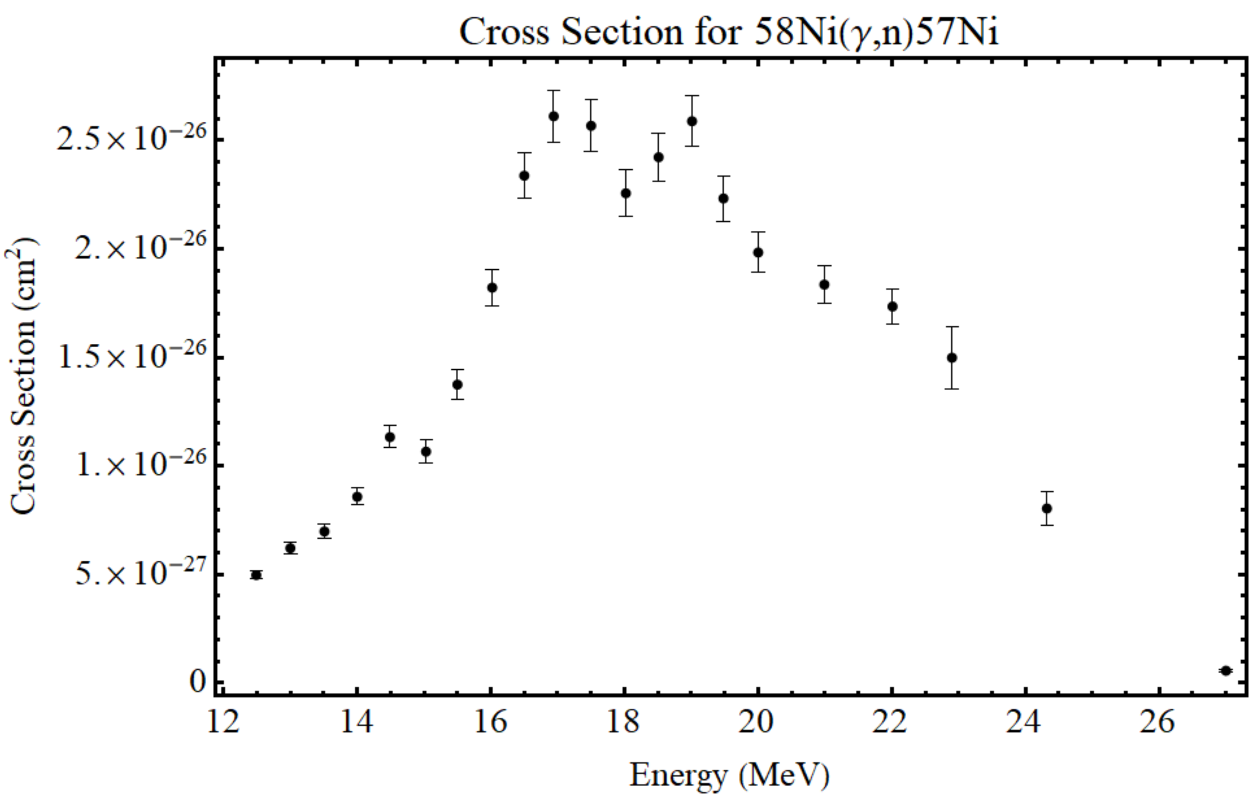

Figure 1: Energy dependent cross section for 58Ni(γ,n)57Ni [1].

In regards to the photo-neutron converter, both tungsten and zinc have a significant (γ,n) cross section. Once the bremsstrahlung photons are produced, they interact with tungsten and zinc to then produce high energy (fast) neutrons. Thus, by the use of bremsstrahlung radiation and photo-nuclear interactions, the PNC has effectively converted incoming electrons from the linac into photons and neutrons. These photons and neutrons can then interact with the gold and nickel foils, producing radioactive isotopes whose activity can be measured and then used to calculate particle flux.

Radioactive Isotope Activation and Decay 1.4

As the gold and nickel foils are irradiated with photons and neutrons from the PNC, the unstable isotopes of gold, nickel, and cobalt are produced due to nuclear interactions. Reactions measured in this work can be seen in Table 1.

Table 1: List of reactions measured using PAA or NAA on the gold and nickel foils [6].

Reaction	**Half Life**	**Decay Energy (keV)**	**Rel. Intensity (%)**	**Decay Mode**
197Au(γ,n)196Au	6.17 days	355.7	87	ε: 93.0
197Au(n,γ)198Au	2.69 days	411.8	95.63	β-: 100
58Ni(γ,n)57Ni	35.6 hours	1377.6	81.7	β+: 100
58Ni(γ,2n)56Ni	6.1 days	811.85	86	ε: 100
60Ni(γ,np)58Co	70.9 days	810.8	99.45	ε: 100
58Ni(n,p)58Co	70.9 days	810.8	99.45	ε: 100

Before irradiation begins, it is assumed that the foils have no radioactive isotopes present. Once particles begin to irradiate a sample, the number of existing radioactive nuclei present in a foil is given by Equation (1).

$$K(t_{irr}) = \frac{VT}{\lambda}(1 - e^{-\lambda t_{irr}}) \tag{1}$$

Where K is the number of radioactive nuclei, V is the volume of the foil (cm^3), λ is the decay constant (1/s), t_{irr} is the total irradiation time (s), and T is the transmutation rate ($1/s{\cdot}cm^3$). The decay constant is dependent on the half-life of the radioactive material, as seen in Equation (2).

$$\lambda = \frac{ln2}{t_{1/2}} \tag{2}$$

Where $t_{1/2}$ is the half-life. The transmutation rate is the rate at which a nuclear reaction occurs, and is dependent on the nuclear cross section of the reaction, and the flux distribution, which is given by Equation (3).

$$T = \frac{N_A \rho}{A_m} \int \sigma(E) \Phi(E) dE \tag{3}$$

Where N_A is Avogadro's Number (mol^{-1}), ρ is the density of the material (g/cm^3), A_m is the atomic mass of the material (u), σ is the cross section (cm^2) and Φ is the differential particle flux ($1/s{\cdot}cm^2{\cdot}MeV$). The purpose of this work is to determine the particle flux distribution, and since Φ is inside an integral and multiplied by the cross section, the shape of this function can be determined using a Monte Carlo simulation. Once the shape is determined, the function can be normalized by a constant in order to match experimental results.

Once the irradiation ends, the foils begin to decay. From here, the number of existing radioactive nuclei present follows the decay law, or Equation (4).

$$K(t) = K(t_{irr})e^{-\lambda t} \tag{4}$$

It is possible to write this in decays per second, also known as activity. This can be seen in Equation (5).

$$A(t) = \lambda K(t) = \lambda K(t_{irr})e^{-\lambda t} \tag{5}$$

Once the activity of a foil is known, it is possible to calculate the number of decays expected over a given time period. This value can be compared to an experimental measurement of the sample's activity. To numerically solve for the number of decays over a given time period, C, the activity needs to be integrated with respect to time. This is visualized in Equation (6).

$$C = \int_{t_{start}}^{t_{end}} A(t)dt = \lambda K(t_{irr}) \int_{t_{start}}^{t_{end}} e^{-\lambda t}dt \tag{6}$$

Photon and Neutron Activation Analysis 1.5

There are multiple methods by which a radioactive isotope can decay, some including electron capture and beta decay. These are recognized as decay modes. When these processes occur, a photon is released with a characteristic energy. This photon energy can be measured using a photon spectrometer, and is one piece of evidence that the specific isotope exists in a material. A measurement of the half-life is the second piece of evidence to unequivocally identify the isotope. This technique is known as photon or neutron activation analysis, depending on which particle activated the sample. With any of these decays, there is a term known as the relative intensity. The relative intensity is the intensity of a specific characteristic photon, and in other terms, is the percentage of time a characteristic photon is included in a decay. Some example relative intensities, characteristic photon energies, and decay modes used in this work can be seen in Table 1.

High Purity Germanium Detectors 1.6

A common detector used in PAA/NAA is a High Purity Germanium Detector (HPGe). Germanium is a semiconductor, and therefore has a band gap. When the characteristic photons from the decaying isotopes hit the germanium crystal, there is a possibility that the photon interacts with the electrons, giving them sufficient energy to cross the band gap making electron-hole pairs. The electron-hole pairs produce an electrical signal that is measured by an analog digital converter (ADC). Since the number of electron-hole pairs depends on the energy of the characteristic photon, the given energy is proportional to the measured electrical signal. Subsequently different reactions have photons with different characteristic energies and radioactive half-lives making it possible to distinguish between decaying isotopes. Data taken from a nickel foil in this work using a HPGe can be seen in the photon energy spectrum shown in Figure 2.

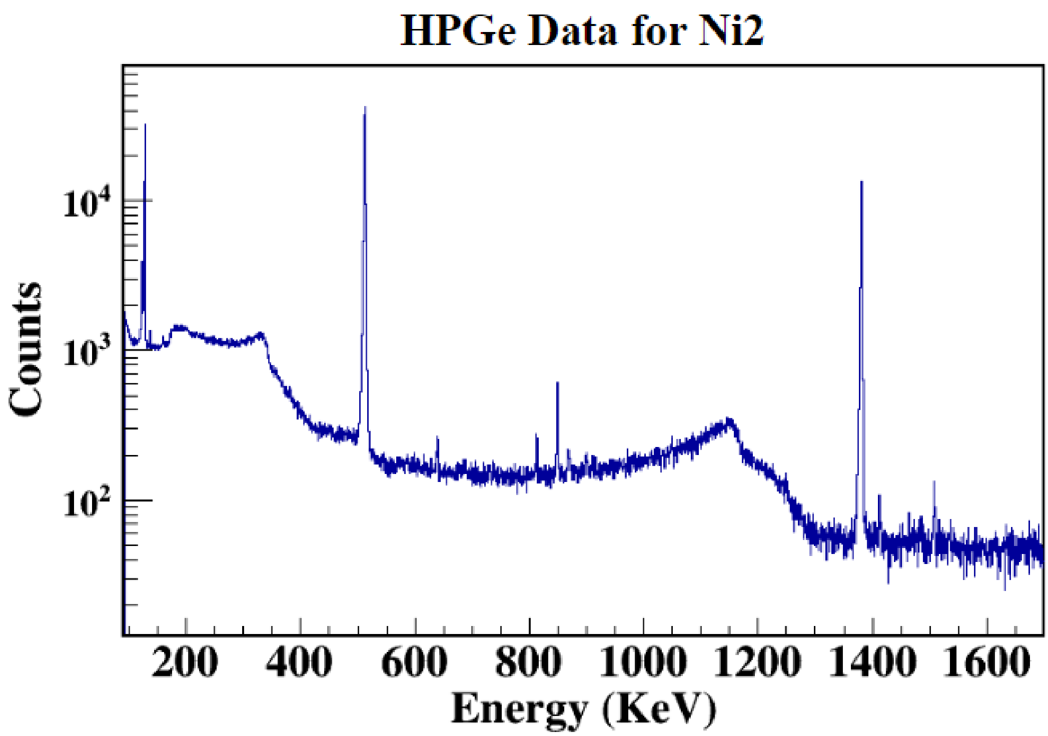

Figure 2: HPGe data from an irradiated nickel sample.

From Figure 2, characteristic photons were measured from decaying isotopes in the nickel foil as seen by the spikes in the histogram. To change channel number to energy, the HPGe first needs to be calibrated with a known radiation source. Once the detector is calibrated, it is clear which characteristic photons are being measured.

The number of decays measured can be found by taking the total number of counts under a desired peak. To accomplish this, it is common practice to fit the peak to a Gaussian probability distribution. The Gaussian probability distribution is seen in Equation (7).

$$G(x) = C_o e^{-\frac{1}{2}(\frac{x-M}{\sigma})^2} \qquad (7)$$

Where C_o, M, and σ are the free parameters of the distribution. Once the peak is fit to a Gaussian probability distribution, the number of decays can be found by integrating the fit over all space. This integral reduces to Equation (8).

$$C = \sqrt{2\pi}\sigma C_o \qquad (8)$$

Thus, once the free parameters of the fit are found, it is possible to experimentally determine the activity of different radioactive isotopes in a foil using a high purity germanium detector and photon or neutron activation analysis.

HPGe Detector Efficiency 1.7

In general, a HPGe will not be able to measure every characteristic photon decay that occurs within a radioactive isotope. This is due to detector efficiency. In this case there are two types of detector efficiency, geometric and intrinsic. The product of these two efficiencies creates the total detector efficiency for a given setup.

Geometric efficiencies can be calculated based on the size of the germanium crystal in the detector and the distance the sample is from the detector. This is known as the solid angle and has units of steradians. The calculation of the solid angle using a point source approximation can be seen in Equation (9).

$$\Omega = \frac{\pi r^2}{d^2} \qquad (9)$$

Where r is the radius of the germanium crystal (cm) and d is the distance the sample is from the detector (cm). The radioactive foils in this work are treated as isotropic sources. This means they can emit their characteristic photons into any direction. In other words, the characteristic photons are emitted into 4π steradians. Therefore, the geometric efficiency is just the ratio of the detector solid angle, Equation (9), over 4π steradians. This can be visualized in Equation (10).

$$G_{eff} = \frac{r^2}{4d^2} \qquad (10)$$

Intrinsic efficiency is a property of the detector itself. Since particle interactions are probabilistic, not every characteristic photon that hits the detector will produce a signal. Intrinsic efficiencies are also energy dependent, so different characteristic photons have different intrinsic efficiencies for a detector. To determine the intrinsic efficiency distribution, sources with known activity must be used and measured using the HPGe. Since the source activity is known, the intrinsic efficiency is the ratio of the measured activity over the source activity. Since the detector is still at a given solid angle away from the source, the geometric efficiency term must be included as well. The calculation of the intrinsic efficiency can be seen in Equation (11).

$$I_{eff} = \frac{A(t)_{measured}}{A(t)_{known} \cdot G_{eff}} \qquad (11)$$

Since the intrinsic efficiency is an energy dependent distribution, it is important to calculate the intrinsic efficiency with varying characteristic photon energies from different sources. For this work, employees at the IAC had previously determined the intrinsic efficiency of the detector at various solid angles. The data for the distribution used to calculate the intrinsic efficiency in this experiment can be seen in Table A 1.

With detector efficiencies known, it is possible to numerically solve for the number of decays expected while using a HPGe. This involves a modification to Equation (6) including the relative intensity (R_I) of the characteristic photon, geometric efficiency, and intrinsic efficiency. This modification is shown in Equation (12).

$$C = R_I G_{eff} I_{eff} \lambda K(t_{irr}) \int_{t_{start}}^{t_{end}} e^{-\lambda t} dt \qquad (12)$$

The last thing to consider when using a HPGe is dead time. When a characteristic photon interacts with the HPGe and produces a signal, it takes time for the detection system to reset and measure another signal. This is known as dead time. Logically, the higher the activity of the source, the more time the detector spends counting, thus increasing the overall dead time. The actual time that the HPGe was available to take measurements is known as live time. For calculation purposes, it is important to use the live time of the detector, which is just the difference in total time and dead time. In this work, the total time, live time, and dead time were given by the data acquisition system (DAQ) used during the experiment, and the live time was used for all calculations.

MCNP 1.8

As mentioned in Section 1.4, to determine the shape of the photon and neutron flux distributions a Monte Carlo simulation was needed. This work utilizes Monte Carlo N-Particle Transport (MCNP) developed by Los Alamos National Laboratory to produce the flux distributions [7]. MCNP utilizes the probabilistic interactions defined by cross sections to determine the particle transport within a given geometry. With MCNP, it is possible to build the experimental geometry and introduce source particles at a given energy. In this case, the electron beam, PNC, and target foils were created and simulated using source parameters that matched the particle accelerator experiment.

An MCNP input file is composed of three sections: cell cards, surface cards, and data cards. Cell cards define the inside of surfaces created in the geometry. The cell cards indicate the type of material inside a surface, and the density of that material. Surface cards define the shape of the geometry and provide boundaries for the cells. With MCNP, it is possible to create surfaces defined by equations, planes, and macrobodies. The largest section is the data card sections, which includes everything else relevant for a given simulation. In this work, the data card section defines materials, particle energy cutoffs, electron source data, and tallies. A copy of the MCNP script used in this work can be seen in Figure A 1.

Tallies are required in order to produce the neutron and photon flux distributions used in this work. In the simulation, an F4 tally was used on the gold and nickel foil cells, which returns the particle flux of the selected cell. MCNP produces flux in units of source particle$^{-1}\cdot$cm^{-2}. In order to translate these values to actual flux (1/s$\cdot$cm^{2}), the electron rate (e^{-}/s) must be determined from the particle accelerator used during the experiment. Multiplying MCNP flux by a particle accelerator's electron rate will produce the simulated particle flux values. In order to get a flux distribution, energy bins were defined ranging from 0.1 MeV to 40 MeV.

Included with MCNP results are statistical errors for the calculated values. These statistical errors are printed as a fractional uncertainty, or percentage of the calculated value. With any Monte Carlo simulation, these errors reduce in magnitude if more source particles are input. However, including more source particles increases the runtime of the simulation, which can cause a runtime error based on the quality of the machine running the code. One method to reduce the runtime for a given simulation is to introduce a particle energy cutoff. For the simulations in this work, an Idaho State University cluster server was used (Thorshammer), which allowed for 1×10^9 source particles to be simulated before hitting a runtime error. With this knowledge, energy bins for the flux tallies were selected in such a way that the statistical errors for the particle flux were significantly less than the systematic errors of the experiment. This included introducing a particle energy cutoff of 0.1 MeV.

Experimental Procedure 2

On December 22, 2020, a 40 MeV linac and a tungsten zinc PNC were used at the Idaho Accelerator Center to irradiate gold and nickel foils. The beam was turned on at 10:10am and off at 12:37pm with a 12-minute within the interval. Consequently, the total irradiation time for the foils was recorded to be 2.25 hours, or 8100 seconds. Beam parameters used for this experiment can be seen in Table 2.

Table 2: Beam time values for the IAC experiment.

Beam Time Values	
Energy (MeV)	37.5 ± 2.5
Peak Current (mA)	73 ± 7.3
Power (kW)	4.12 ± 0.41
Rep Rate (Hz)	300
Pulse Width (μs)	5
Electron Rate (e^-/s)	$(6.83 \pm 0.35)\times10^{14}$
Start Time	10:10 AM
End Time	12:37 PM
Irradiation Time (s)	8100

Photo-Neutron Converter Design 2.1

The PNC used in this experiment consists of six 0.76mm tungsten cylindrical plates followed by a 1.98cm zinc cylinder held in place by a carbon crucible. The entire PNC was enclosed in steel with an aluminum end cap in order to create a cavity for water to flow and cool the PNC. The actual PNC can be visualized in Figure 3 and simulated geometry from MCNP can be seen in Figure 4. The PNC was placed directly in the beam line in order for the electrons to directly interact with the tungsten plates to produce bremsstrahlung radiation.

Figure 3: PNC at the IAC oriented vertically.

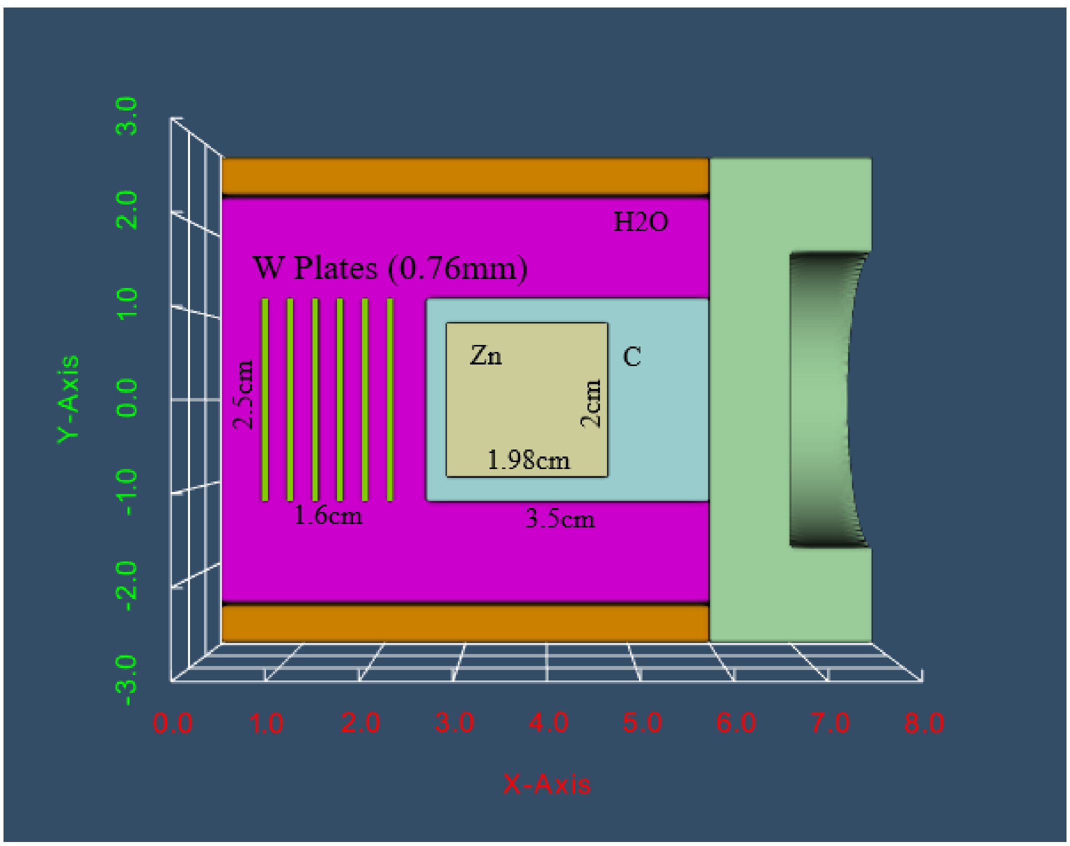

Figure 4: MCNP simulated geometry of the PNC (axes in cm).

Gold and Nickel Foil Placement 2.2

To measure the photon and neutron flux, gold and nickel foils were placed at various distances and angles off of the PNC. Before the foils were placed, the lengths of the foils were measured using a ruler and the mass was taken using a digital scale. The first foil, nickel 1 (Ni1) was placed right after the aluminum end cap of the PNC, directly in the beam line. Gold 1 (Au1), nickel 2 (Ni2), and gold 2 (Au2) were stacked vertically 8.0 ± 0.1 cm away from the start of the PNC. Gold 3 (Au3) was 90^{o} off of the beamline axis, placed 2.2 ± 0.1 cm away from the start of the PNC. All foil values and locations can be seen in Table 3. Pictures of the experimental setup at the end of the beamline can be seen in Figure 5 and Figure 6. MCNP simulated geometry of the experimental setup can be seen in Figure 7.

Table 3: Foil values and geometry.

Foil	**Angle Off Beamline (Degrees)**	**Horizontal Distance from Start of PNC (cm)**	**Area (cm^2)**	**Mass (g)**	**Volume (cm^3)**
Au1	29.6 ± 0.2	8.0 ± 0.1	2.0 ± 0.1	0.1890 ± 0.0005	0.0098 ± 0.0007
Au2	47.3 ± 0.1	8.0 ± 0.1	1.4 ± 0.1	0.1518 ± 0.0005	0.0079 ± 0.0006
Au3	90	2.2 ± 0.1	1.6 ± 0.1	0.1643 ± 0.0005	0.0085 ± 0.0007
Ni1	0	7.0 ± 0.1	4.6 ± 0.2	0.1040 ± 0.0005	0.012 ± 0.0006
Ni2	39.5 ± 0.2	8.0 ± 0.1	4.0 ± 0.1	0.0917 ± 0.0005	0.010 ± 0.0005

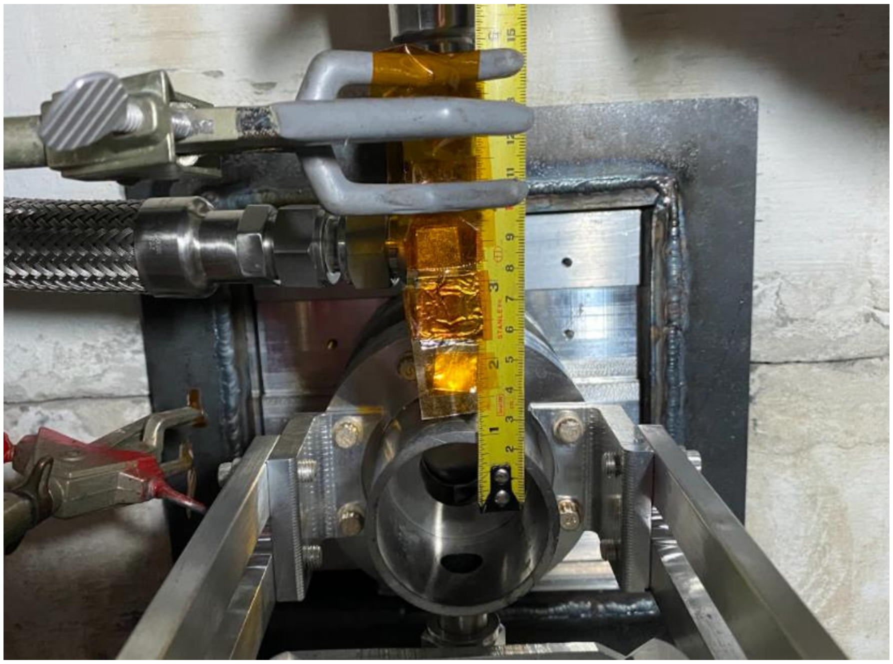

Figure 5: Vertical view of IAC beamline with Au1, Ni2, Au2, and Au3.

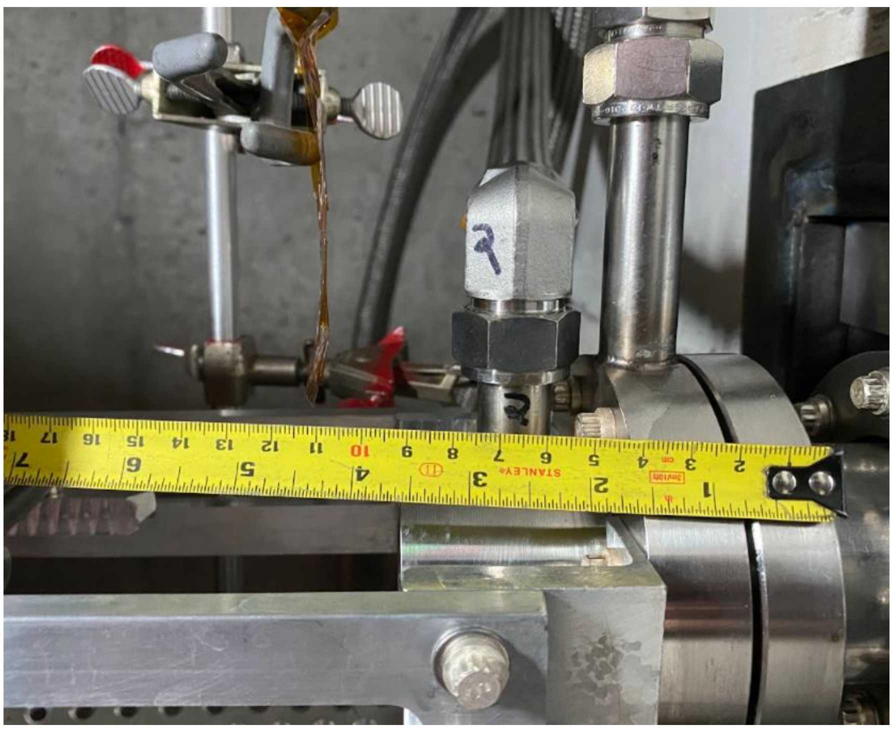

Figure 6: Horizontal view of IAC beamline with Au1, Ni2, and Au2.

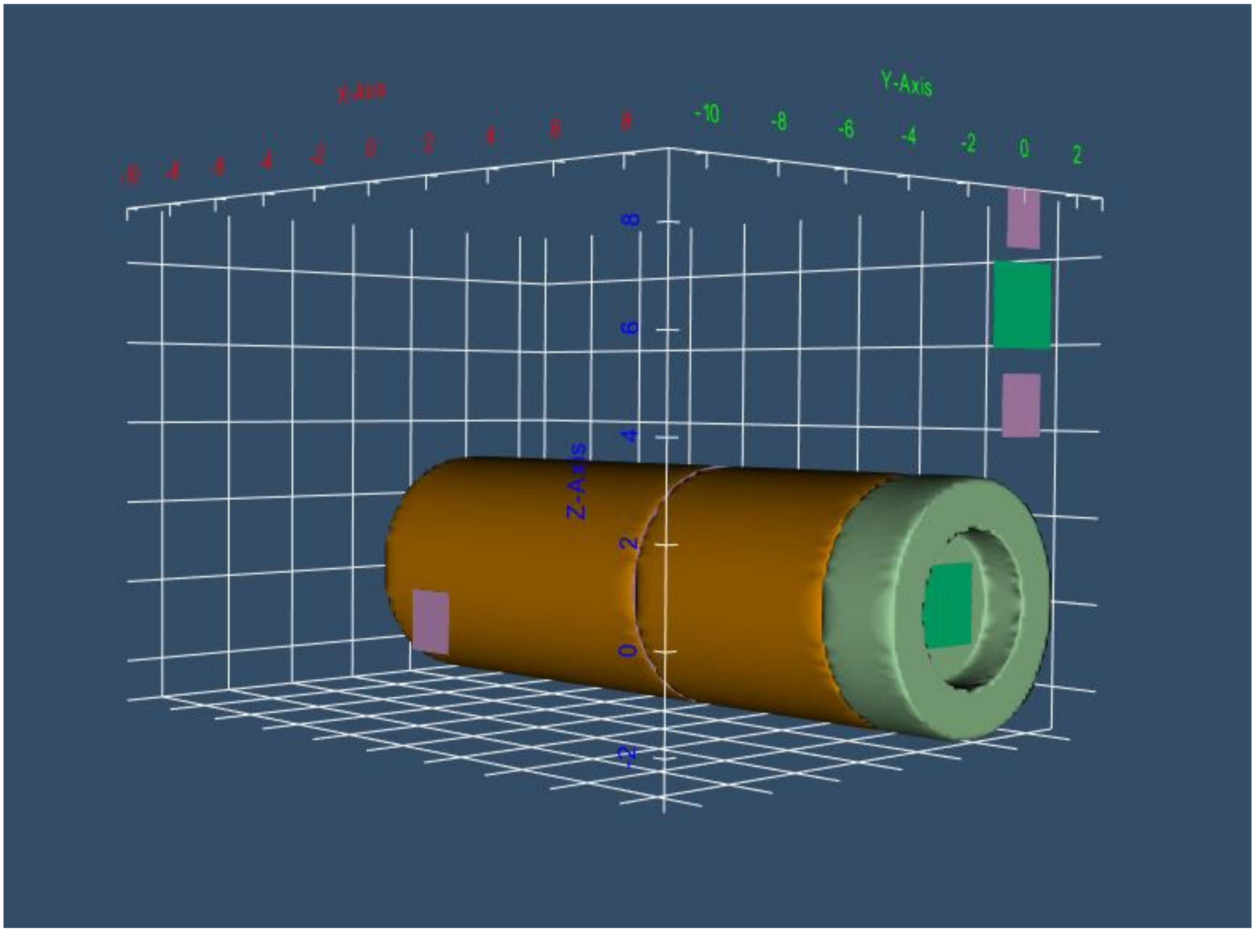

Figure 7: MCNP simulated geometry of the IAC experiment. Gold foils are pink and nickel foils are green.

HPGe Detector Setup 2.3

Once the electron beam was turned off, the foils’ activity was measured using high purity germanium detectors. The IAC has two detectors, detector A (DetA) and detector D (DetD). Based on availability both detectors were used in the experiment. The specifications for detector A and detector D can be seen in Table 4.

Table 4: HPGe specifications for the IAC detectors.

HPGe Specifications	**Detector A**	**Detector D**
Make	Ortec	Canberra
Model	GEM40P4	GC3318
Serial Number	47-TP50314B	8902320
Voltage (V)	4600	2500
Crystal Diameter (mm)	65.7	58

The time and date a foil was measured depended on the activity of the foil, and the reaction being measured. For all tests, the gold foils were measured 16 ± 0.1 cm away from the detector and the nickel foils were measured 8 ± 0.1 cm. These distances were chosen to reduce dead time of the foils for measurements taken on 12/22/2020, and then kept consistent for every measurement following. Each time data was taken, the desired reaction was measured until the statistical uncertainty in the Gaussian distribution peak was less than 1%. Certain foils, like Ni2, were measured multiple times in order to obtain a good measurement for each reaction of interest. For example, referring to Table 1, the half-life of Ni 57 is 35.6 hours, while the half-life of Co 58 is 70.9 days. When the first measurement of Ni2 was made, the activity from Ni 57 was much higher than Co 58, so the Ni 57 peak hit its desired uncertainty much faster than the Co 58 peak. At a later date, once the activity of the Ni 57 peak dropped, a measurement for the Co 58 peak was made until the desired uncertainty was reached. Data filenames along with their corresponding dates can be seen in Table 5. To avoid any issues regarding detector calibration, a calibration measurement was done each new day a foil was to be measured.

Table 5: List of measurements taken on Au and Ni foils.

File	Date	Start Time	Total Time	Live Time	% Dead
Ni2DetA8cmData	12/22/2020	16:33:34	1109.936	1054.439	5
Au2DetA16cmData	12/22/2020	17:02:23	287.61	272.08	5.4
Au3DetA16cmData	12/22/2020	17:16:55	2313.131	2213.666	4.3
Au1DetA16cmData	12/26/2020	14:16:45	719.189	637.467	11.36
Au1DetA16cm_2Data	12/28/2020	15:44:12	475.605	433.91	8.77
Ni2DetA8cm_2Data	12/28/2020	15:54:31	4186.9	4170.8	0.38
Ni1DetD8cmData	1/2/2021	20:09:55	6282.5	5815.3	7.44
Ni2DetD8cm_3Data	1/13/2021	13:19:16	76383.021	76308.3	0.1

Data Analysis 3

Once all the measurements were made, the files were analyzed by a software known as ROOT developed by CERN [8]. ROOT has the capability to plot the histogram data from the HPGe, and fit the desired reaction peaks to a Gaussian probability distribution. Once the free parameters of the fit were known, the number of decays which occurred over the measurement time period was calculated using Equation 8. These values were then compared to simulated results from MCNP using Equation 12.

Multi-Channel Histogram Analysis 3.1

When using ROOT to fit histograms to a Gaussian probability distribution, the free parameters of the fit will change depending on how many channels are chosen to include in the fit. To account for this, three fits were made for each peak using 14, 10, and 8 channels. The number of decays was calculated for each fit using Equation 8, and an average was calculated for the final result. The standard deviation of all three results was also calculated and used as the uncertainty in the measurement. An example of a 14-channel histogram fit can be seen in Figure 8.

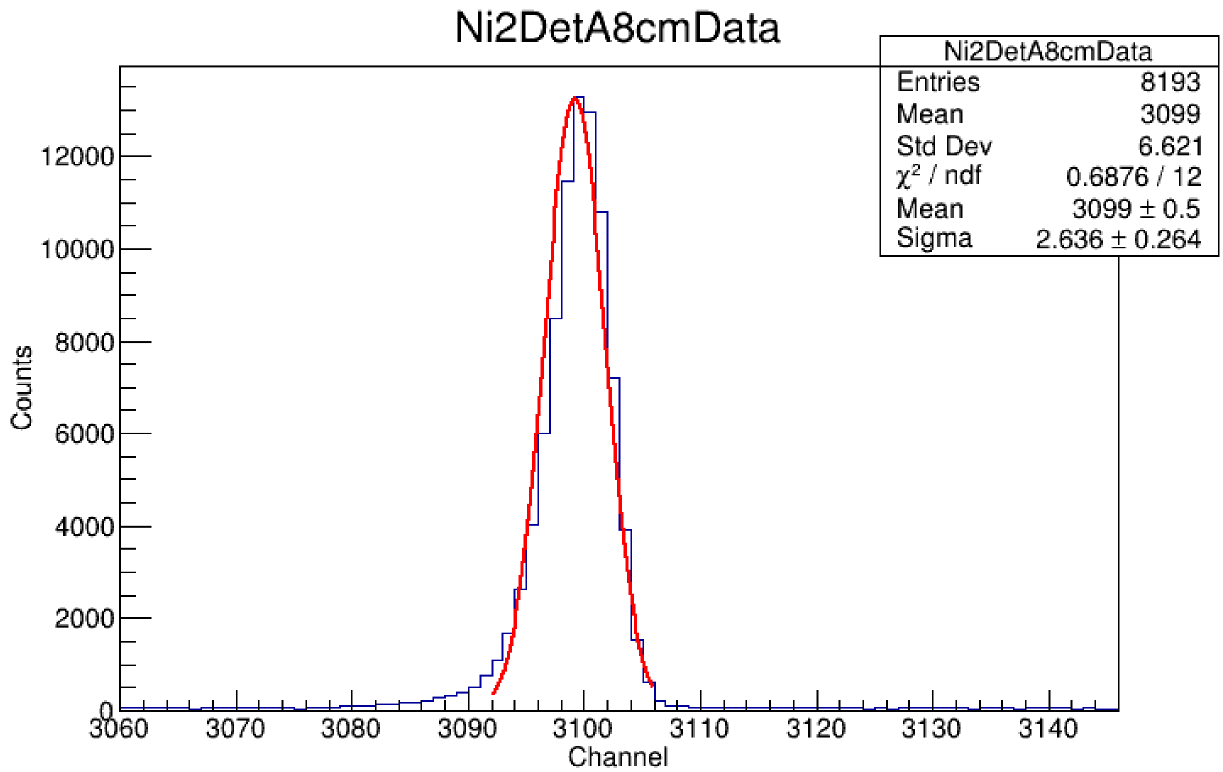

Figure 8: 14-channel fitted data for Ni2 on ROOT.

Photon Flux Normalization 3.2

The first flux distribution analyzed was the photon flux coming off of the PNC. Once the MCNP simulation was completed, the simulated photon flux distributions were normalized by the electron rate from Table 2. Focusing on the nickel foils, the transmutation rate (Equation 3) was calculated using the photon flux from MCNP and the 58Ni(γ,n)57Ni cross section (Figure 1). Once the transmutation rate was calculated, the theoretical number of decays was calculated using Equation 12. These values were compared to the actual experimental results from the ROOT analysis, which can be seen in Table 6 and Table 7.

Table 6: Experimental decays for 58Ni(γ,n)57Ni.

ROOT Analysis 58Ni(γ,n)57Ni	**Counts**	**Uncertainty**	**% Uncertainty**
Ni1DetD8cmData	197180	4513	2
Ni2DetA8cmData	87547	38	0.04
Ni2DetA8cm_2Data	20081	183	0.9

Table 7: Simulated decays for 58Ni(γ,n)57Ni.

MCNP Analysis 58Ni(γ,n)57Ni	**Counts**	**Uncertainty**	**% Difference**	**% Uncertainty**
Ni1DetD8cmData	258574	17015	31	7
Ni2DetA8cmData	116939	7420	34	6
Ni2DetA8cm_2Data	30172	1915	50	6

The results above suggest that MCNP is predicting a larger photon flux than what was measured. To normalize the MCNP results, the simulated decay rate for each foil was plotted with the experimental results. An example of this for Ni2 can be seen in Figure 9. The experimental data was fit to a modified version of Equation 5, which can be seen in Equation 13.

$$A(t) = N_f \lambda K(t_{irr}) e^{-\lambda t} \quad (13)$$

Where N_f is the normalization factor needed for simulated results to match experimental results. For Ni1 and Ni2, the normalization factor was found to be 0.75 for both foils in regards to photon flux. The results of this process for Ni2 can be seen in Figure 10.

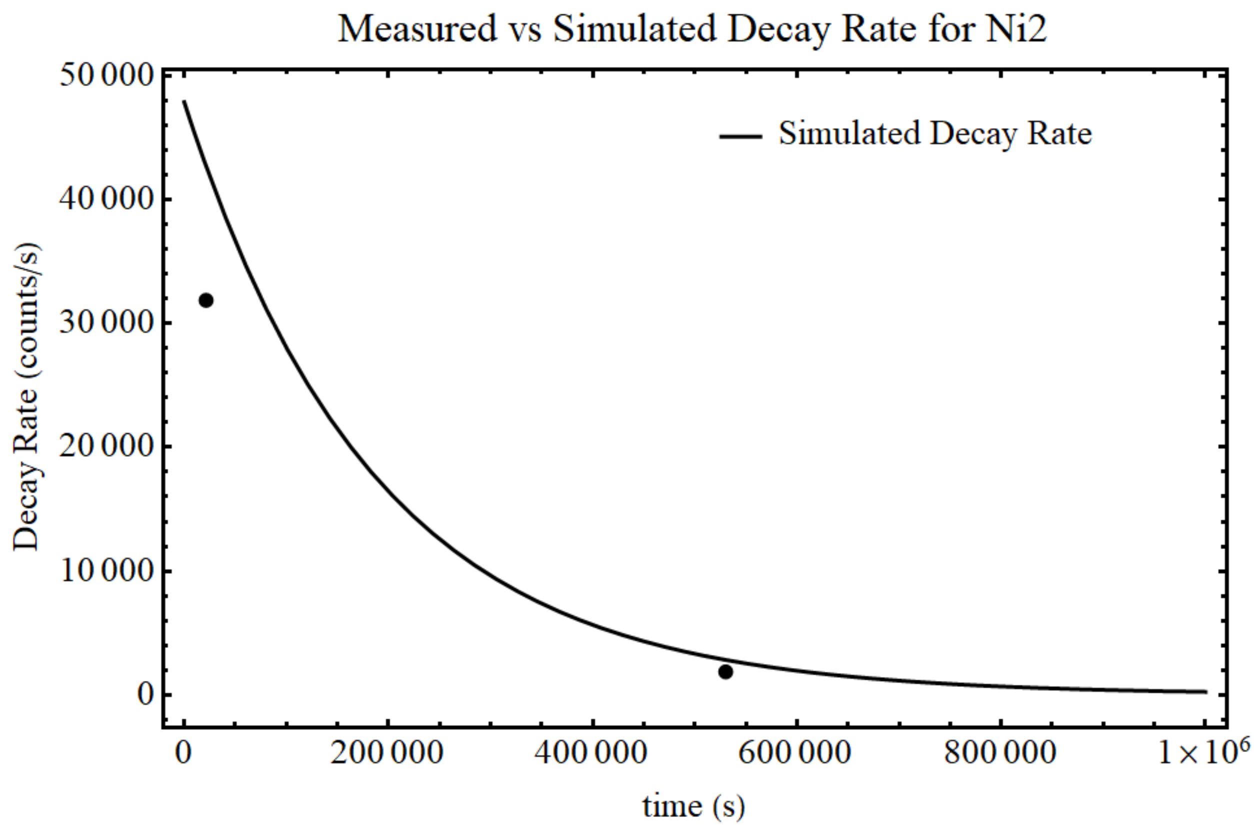

Figure 9: Comparison of simulated decay rate against Ni2 measurements. Data points are experimental measurements.

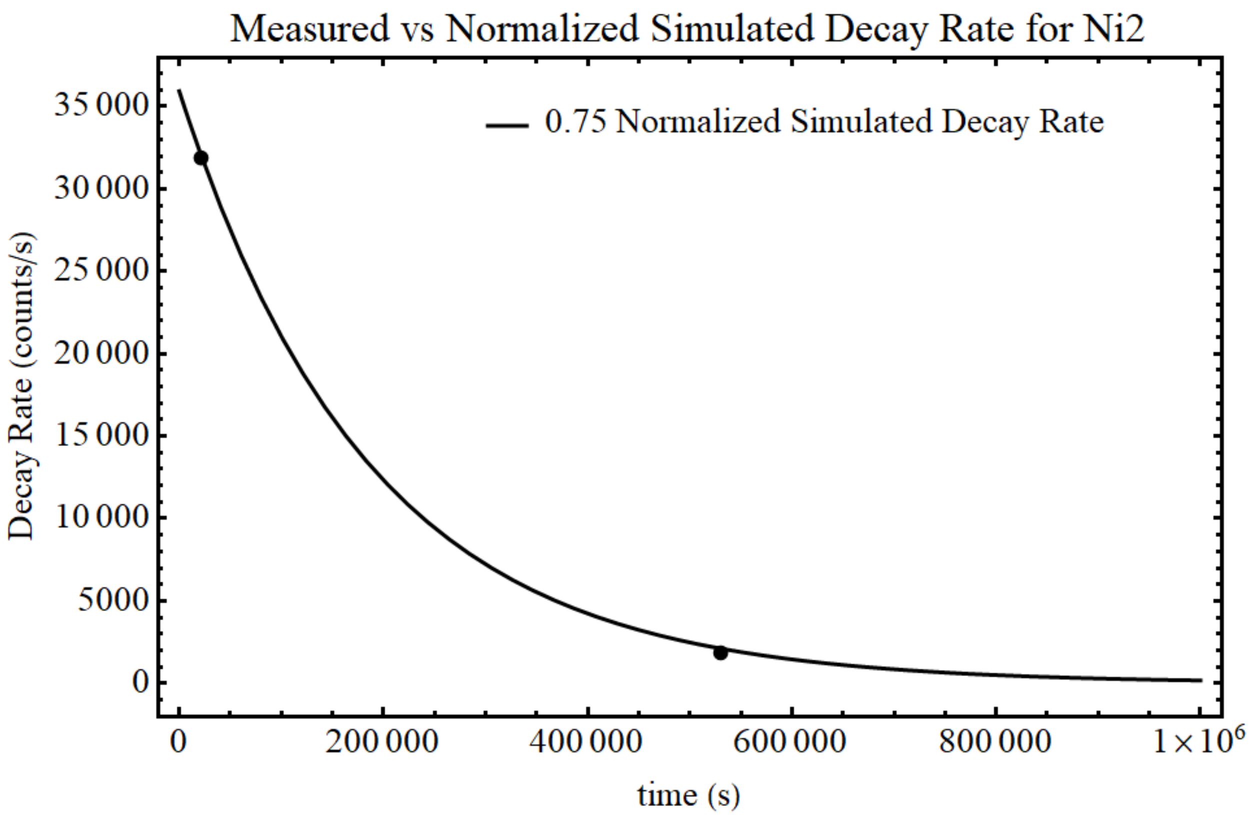

Figure 10: Comparison of normalized decay rate against Ni2 measurements. Data points are experimental measurements.

This same procedure was followed for gold, utilizing the reaction 197Au(γ,n)196Au. The experimental and simulated results for gold can be viewed in Table 8 and Table 9. In this analysis, it is assumed that MCNP is correct in the angle distribution of the flux due to its Monte Carlo analysis method. Therefore, each foil should have the same normalization factor. To accomplish this, a weighted average of the normalization factor from each foil was taken. Each normalization factor and the weighted average can be seen in Table 10.

Table 8: Experimental decays for 197Au(γ,n)196Au.

Root Analysis 197Au(γ,n)196Au	**Counts**	**Uncertainty**	**% Uncertainty**
Au1DetA16cmData	510634	13696	3
Au1DetA16cm_2Data	295053	6414	2
Au2DetA16cmData	62602	156	0.2
Au3DetA16cmData	67666	1533	2

Table 9: Simulated decays for 197Au(γ,n)196Au.

MCNP Analysis 197Au(γ,n)196Au	**Counts**	**Uncertainty**	**% Difference**	**% Uncertainty**
Au1DetA16cmData	698314	108192	37	15
Au1DetA16cm_2Data	377145	58432	28	15
Au2DetA16cmData	64717	10232	3	16
Au3DetA16cmData	71836	20718	6	29

Table 10: Normalization factor for photon flux.

Foil	**Photon Normalization Factor**	**Weighted Average**	**Uncertainty**
Ni1	0.75	0.75	0.03
Ni2	0.75		
Au1	0.67		
Au2	0.92		
Au3	0.94		

Once the normalization factor was found, it was applied to the simulated photon flux distribution from MCNP. The results of this correction can be seen in Table 11 and Table 12. The simulated photon flux distribution plotted with the normalized photon flux distribution for nickel and gold can be visualized in Figure 11 and Figure 12 respectively.

Table 11: Normalized simulated decays for 58Ni(γ,n)57Ni.

Normalized MCNP Analysis 58Ni(γ,n)57Ni	**Counts**	**Uncertainty**	**% Difference**	**% Uncertainty**
Ni1DetD8cmData	194563	15159	-1	8
Ni2DetA8cmData	87991	6682	1	8
Ni2DetA8cm_2Data	22703	1724	13	8

Table 12: Normalized simulated decays for 197Au(γ,n)196Au.

Normalized MCNP Analysis 197Au(γ,n)196Au	**Counts**	**Uncertainty**	**% Difference**	**% Uncertainty**
Au1DetA16cmData	525443	84309	3	16
Au1DetA16cm_2Data	283781	45533	-4	16
Au2DetA16cmData	48696	7963	-22	16
Au3DetA16cmData	54053	15752	-20	29

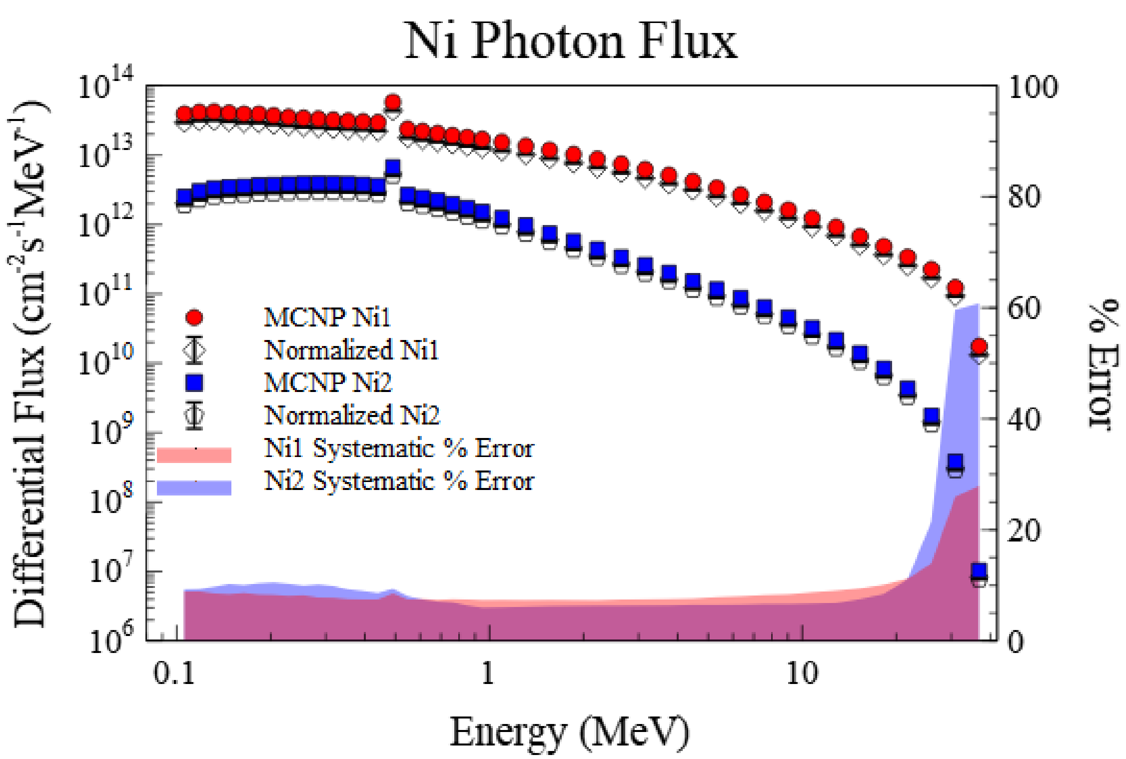

Figure 11: Photon flux distribution for nickel foils.

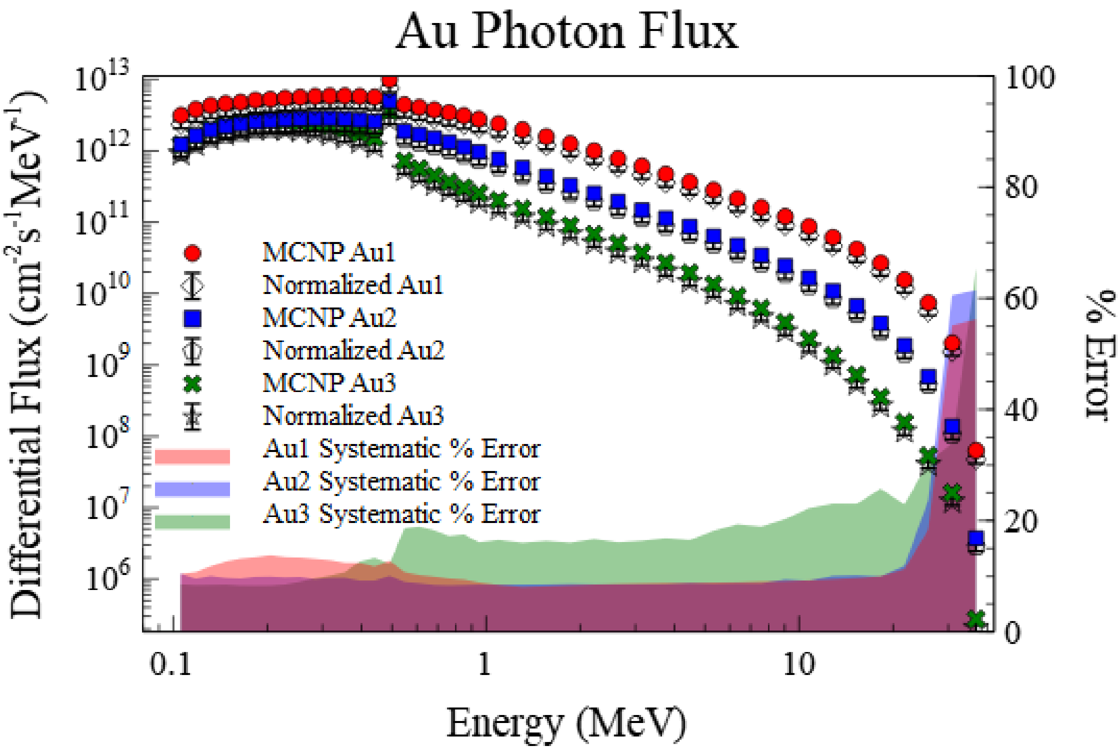

Figure 12: Photon flux distribution for gold foils.

Neutron Flux Normalization 3.3

The second flux distribution analyzed was the neutron flux coming off of the PNC. The procedure in which the neutron flux distribution was found is similar to Section 3.2, however more than one reaction needed to be considered when calculating the simulated number of decays from the MCNP results. Looking at Table 1, the reaction used to determine the neutron flux for the nickel foils was 58Ni(n,p)58Co, which produces a characteristic photon at 810.8 keV. The reactions 58Ni(γ,2n)56Ni and 60Ni(γ,np)58Co produce characteristic photons at 811.85 keV and 810.8 keV respectively. Since all of these reactions produce a characteristic photon indistinguishable on a HPGe, the 58Ni(γ,2n)56Ni and 60Ni(γ,np)58Co reactions must be included in the calculation in order to match experimental results using PAA and NAA. Since the two reactions 58Ni(γ,2n)56Ni and 60Ni(γ,np)58Co are triggered by incident photons, the normalized photon flux distribution results from Figure 11 can be used to calculate the transmutation rate (Equation 3). The calculated results of these two photon reactions for the number of decays was added onto the simulated results for the 58Ni(n,p)58Co reaction. From there, a normalization factor was found using the same procedure as Section 3.2. The results for this process can be seen in Table 13, Table 14, Table 15, Table 16, and Figure 13.

Table 13: Experimental decays for 58Ni(n,p)58Co, 58Ni(γ,2n)56Ni, and 60Ni(γ,np)58Co.

Root Analysis	**Counts**	**Uncertainty**	**% Uncertainty**
Ni1DetD8cmData	141930	4290	3
Ni2DetD8cm_3Data	31140	577	2

Table 14: Simulated decays for 58Ni(n,p)58Co, 58Ni(γ,2n)56Ni, and 60Ni(γ,np)58Co.

MCNP Analysis	**Counts**	**Uncertainty**	**% Difference**	**% Uncertainty**
Ni1DetD8cmData	105062	24303	-26	23
Ni2DetA8cm_3Data	27019	9097	-13	34

Table 15: Normalization factor for neutron flux.

Foil	**Neutron Normalization Factor**	**Weighted Average**	**Uncertainty**
Ni1	1.35	1.3	0.2
Ni2	1.15		

Table 16: Normalized simulated decays for 58Ni(n,p)58Co, 58Ni(γ,2n)56Ni, and 60Ni(γ,np)58Co.

Normalized MCNP Analysis	**Counts**	**Uncertainty**	**% Difference**	**% Uncertainty**
Ni1DetD8cmData	111747	25093	-21	22
Ni2DetA8cm_3Data	33942	13120	9	39

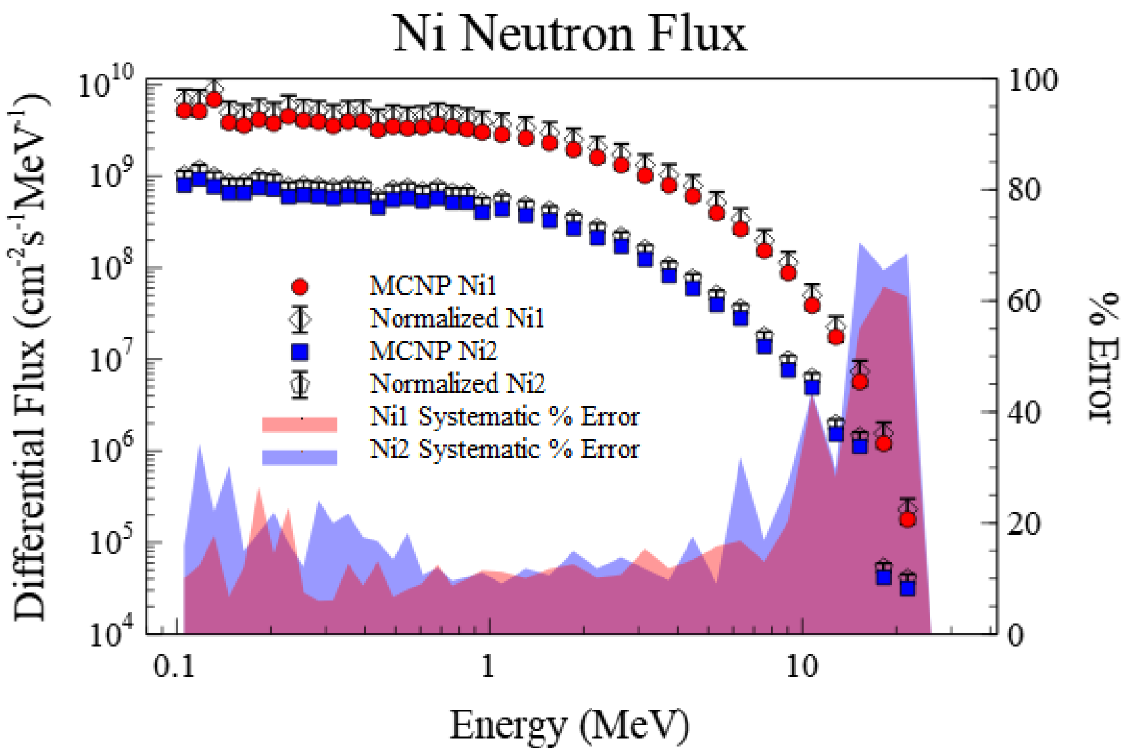

Figure 13: Neutron flux distribution for nickel foils.

Performing the analysis method used in this work for the neutron flux on the gold foils breaks down due to computer computation time. In examining Table 1, the reaction 197Au(n,γ)198Au decays with a characteristic photon that can be measured using a HPGe. This experimental measurement could be compared to MCNP results using the same methods as the other reactions, however the cross section for 197Au(n,γ)198Au has an energy range below what MCNP can produce within reasonable statistical uncertainties. As mentioned previously, MCNP runtime is limited by the computer. In this work, the flux distributions are limited to an energy range of 0.1 MeV and above. From the National Nuclear Data Center, the threshold for the reaction 197Au(n,γ)198Au begins at 0 MeV, so the calculated transmutation rate using the MCNP flux distribution and Equation (3) is not an accurate representation of the actual transmutation rate [6]. Consequently, normalizing the MCNP flux distribution to match experimental data would yield inaccurate results.

Error Analysis 4

The main sources of error in this work are the systematic errors in the experimental design and the uncertainties taken from the cross sections that were used. All statistical errors were significantly reduced to be below the systematic errors by maximizing the MCNP runtime and by taking HPGe measurements with significant live times. All known sources of error were propagated through each calculation using the error analysis methods described in *An Introduction to Error Analysis* by John R. Taylor [9].

Experimental Uncertainties 4.1

Systematic experimental uncertainties arise from the linac, experimental geometry, and detector geometry. The geometries and source information used in the MCNP script were taken from the experimental measurements made at the end of the beam line. The measurements for the geometry were taken using a standard tape measure and an assumed systematic uncertainty of 0.1 cm. The uncertainty in the beam energy was provided by the beam operator at the IAC, and yielded a value of 2.5 MeV. In order to determine how these uncertainties affected the flux distribution, multiple MCNP scripts were run with altered geometry at the uncertainty range. The error in the flux distribution was then taken to be the maximum variation between the original geometry and the altered geometries.

The uncertainty in the detector geometry stems from determining the geometric efficiency of the detector. In order to calculate the solid angle, the distance the foils are from the detector must be measured. A systematic uncertainty of 0.1 cm was included in this measurement and propagated throughout the calculations. Along with detector geometry, the measured volume of the foils has a systematic uncertainty as well. The foil lengths were measured with a ruler and the mass was measured using a digital scale. The ruler had an assumed uncertainty of 0.05 cm and the scale had an assumed uncertainty of 0.0005 g. These values were included in Equation 1 to contribute to the uncertainty in the number of radioactive nuclei present in a foil. A summarized table of the systematic experimental uncertainties can be seen in Table 17.

Table 17: Systematic experimental uncertainties.

	% Uncertainty
Au1 Volume	7.1
Au2 Volume	7.6
Au3 Volume	8.2
Ni1 Volume	5.0
Ni2 Volume	5.0
Au Detector Distance	0.63
Ni Detector Distance	1.3
Au1 Beamline Distance	1.3
Au1 Beamline Angle	0.68
Au2 Beamline Distance	1.3
Au2 Beamline Angle	0.21
Au3 Beamline Distance	4.5
Au3 Beamline Angle	0.0
Ni1 Beamline Distance	1.4
Ni1 Beamline Angle	0.0
Ni2 Beamline Distance	1.3
Ni2 Beamline Angle	0.51
Beam Energy	6.7

Cross Section Uncertainties 4.2

A large contributor to the uncertainty in this work is the error associated with the cross section data available. This varies depending on the reaction, with some cross sections having higher uncertainties than others. If an available cross section did not provide uncertainties, a 10% uncertainty was assumed for this work. Overall, the 58Ni(γ,n)57Ni cross section had the lowest uncertainty, which yielded the smallest variation in results for the photon flux distribution in the nickel foils. 58Ni(γ,2n)56Ni on the other hand had large uncertainties, which led to a large variation in the neutron flux distribution in the nickel foils. With that, the cross section for the reaction 60Ni(γ,np)58Co has not been measured experimentally, and the only available cross section for this reaction was generated using a simulation. Because of this, the assumed uncertainty for the 60Ni(γ,np)58Co cross section was 100%. This affected the uncertainty in the neutron flux distribution for the nickel foils. A summarized table with total fractional uncertainty for each flux distribution can be seen in Table 18.

Table 18: Summarized flux fractional uncertainties.

% Uncertainty								
Foil	**Reaction**	**Foil Volume**	**Transmutation Rate**	**Detector Solid Angle**	**Simulated Total**	**Normalization Factor**	**Total With Normalization**	**Total Flux % Uncertainty**
Ni1 Photon Flux	58Ni(γ,n)57Ni	4.7	4.0	2.4	6.6	4.1	7.8	7.8
Ni2 Photon Flux	58Ni(γ,n)57Ni	4.9	3.3	2.4	6.3	4.1	7.6	7.6
Au1 Photon Flux	197Au(γ,n)196Au	7.1	14	1.2	15	4.1	16	16
Au2 Photon Flux	197Au(γ,n)196Au	7.6	14	1.2	16	4.1	16	16
Au3 Photon Flux	197Au(γ,n)196Au	8.2	28	1.2	29	4.1	29	29
Ni1 Neutron Flux	58Ni(n,p)58Co	4.7	12	2.4	13	19	23	22
	60Ni(γ,np)58Co	4.7	22	2.4	N/A	4.1	23	
	58Ni(γ,2n)56Ni	4.7	41	2.4	N/A	4.1	41	
Ni2 Neutron Flux	58Ni(n,p)58Co	4.9	37	2.4	38	19	42	39
	60Ni(γ,np)58Co	4.9	25	2.4	N/A	4.1	26	
	58Ni(γ,2n)56Ni	4.9	50	2.4	N/A	4.1	51	

Results 5

The purpose of this work was to determine the photon and neutron flux distribution at different angles off of a tungsten photo-neutron converter at the Idaho Accelerator Center. This was accomplished by using photon and neutron activation analysis on radioactive foils and flux distributions generated by MCNP. The results for the photon flux through the nickel and gold foils can be seen in Figure 11 and Figure 12 respectively. While the neutron flux through the gold foils was unable to be determined due to computer computational time, the neutron flux through nickel can be visualized in Figure 13. All of the raw flux data can be found in the appendix, starting at Table A 2. From these results, given a linac beam energy of 37.5 ± 2.5 MeV and a peak current of 73 mA, there is a minimum expected neutron rate of $(1.9 \pm 0.4)\times10^{12}$ n/s with neutron energies greater than 0.1 MeV from the PNC.

If this work were to be improved upon, it would be desirable to only use nickel foils for the photon flux given the low uncertainty in the 58Ni(γ,n)57Ni cross section. To improve the neutron flux distribution, it would be sensible to find a different foil material other than nickel that does not have competing characteristic photons from different nuclear interactions. Gold would be a solution if access to a more computational power was available.

Bibliography

[1] H. Utsunomiya, T. Renstrøm, G. M. Tveten, S. Goriely, S. Katayama, T. Ari-izumi, D. Takenaka, D. Symochko, B. V. Kheswa, V. W. Ingeberg, T. Glodariu, Y.-W. Lui, S. Miyamoto, A. C. Larsen, J. E. Midtbø, A. Görgen, S. Siem, L. Crespo Campo, M. Guttormsen, S. Hilaire, S. Péru, and A. J. Koning. Photoneutron cross sections for Ni isotopes: Toward understanding (n, γ) cross sections relevant to the weak s-process nucleosynthesis. *Phys. Rev.* C 98, 2018.

[2] C. Plaisir, F. Hannachi, F. Gobet, M. Tarisien, M.M. Al´eonard, V. M´eot, G. Gosselin, P. Morel, and B. Morillon. Measurement of the 85Rb(γ,n)84mRb cross-section in the energy range 10–19 MeV with bremsstrahlung photons. *Eur. Phys. J. A 48:68*, 2012.

[3] S. C. Fultz, R. A. Alvarez, B. L. Berman, and P. Meyer. Photoneutron cross sections of 58Ni and 60Ni. *Phys. Rev. C 10 608*, 1974.

[4] T. Kawano, A. Kahler, L. Leal. Evaluated Nuclear Data File (ENDF). *Nucl. Data Sheets 148*, *1*, 2018.

[5] A. J. Koning. Evaluated Nuclear Data File (ENDF). *TENDL*, 2019.

[6] Chart of Nuclides. *National Nuclear Data Center, Brookhaven National Laboratory.* URL https://www.nndc.bnl.gov/nudat3/

[7] T. Goorley, et al., "Initial MCNP6 Release Overview", Nuclear Technology, 180, pp 298-315 (Dec 2012).

[8] Rene Brun and Fons Rademakers, ROOT – An Object Oriented Data Analysis Framework, Proceedings AIHENP'96 Workshop, Lausanne, Sep. 1996, Nucl. Inst. & Meth. In Phys. Res. A 389 (1997) 81-86. Release v6.22.00.

[9] J. Taylor. *An Introduction to Error Analysis: The Study of uncertainties in Physical Measurements*. University Science Books, 1982.

[10] Christian Segebade, Hans-peter Weise, and George J. Lutz, *Photon Activation Analysis*, Walter-de Gruther, Berlin, New York, 1988, p. 20-26.

[11] Robert R. Greenberg, Peter Bode, Elisabete A. De Nadai Fernandes, *Neutron activation analysis: A primary method of measurement*, Spectrochimica Acta Part B: Atomic Spectroscopy, Volume 66, Issues 3–4, 2011, p. 193-241.

[12] Mayir Mamtimin, *A Study of Electron Accelerator Based Photon & Neutron Production and Applications to Nuclear Transmutation Technologies*, Idaho State University, 2014.

Appendix

IAC Experiment Simulation 12_20_20
c
c ++
c
c PROBLEM DESCRIPTION
c
c The new style chamber and Zn target in Jack
c Target: Tungsten alloy Radiator 6 plates
c Zn Target water surrounds it
c
c ++
c
c ++
c
c CELLS
c
c Comment (if any) Applies to Following Cell
c
c ++
c The world is cell 1
1 0 1
c Vacuum Beam Pipe
2 486 -7.92 -2 3 -5 4
c Beam vacuum inside of pipe
3 0 4 -3 -5
c Titanium window electron beam enters
4 498 -4.54 5 -6 -2
c W disk converters
5 272 -17.1 8 -9 -7
6 272 -17.1 10 -11 -7
7 272 -17.1 12 -13 -7

8 272 -17.1 23 -24 -7
9 272 -17.1 25 -26 -7
10 272 -17.1 27 -28 -7
c No second Titanium window
c Aluminum Endcap
12 283 -2.7 -2 19 -201 202
c converter and target holder
13 486 -7.92 6 -2 3 -19
c Carbon crucible
14 320 -2.2 -7 16 -19 #15
c Zn target
15 273 -7.14 17 -18 -22
c Au foil
151 284 -19.3 -221
152 284 -19.3 -222
153 284 -19.3 -223
c Nickel foil
161 285 -8.9 -211
162 285 -8.9 -212
c Water
16 514 -1 -3 6 -19 #5 #6 #7 #8 #9 #10 #14 #15 #12
c Air
17 204 -0.001225 -1 #2 #3 #4 #5 #6 #7 #8 #9 #10 #13 &
#14 #15 #16 #12 #151 #152 #153 #161 #162
c
c ++
c
c SURFACES
c
c Comment (if any) Applies to Following Surface
c
c ++

1 so 50
c Outside beam pipe
2 cx 3
c Inside beam piep
3 cx 2.5
c End of beam pipe
4 px -10
c Start of electron beam Ti Window
5 px -0.0025 $Ti Window
c End of Ti Window
6 px 0
c Converter and Target Cylinder
7 cx 1.25
c First Converter Plate
8 px 0.5
c End of first converter plate
9 px 0.576
c Start of 2nd comverter plate
10 px 0.806
c End of 2nd converter plate
11 px 0.882
c Start of 3rd converter plate
12 px 1.12
c End of 3rd converter plate
13 px 1.196
C Start of 4th converter plate
23 px 1.426
c End of 4th converter plate
24 px 1.502
c Start of 5th converter plate
25 px 1.732
c End of 5th converter plate
26 px 1.808

c Start of 6th converter plate
27 px 2.038
c End of 6th converter plate
28 px 2.114
c Start of Crucible (.05 "space)
16 px 2.518
c inside of Cruc, (2.5 mm base) Start of Zn
17 px 2.768
c End of Zn
18 px 4.75
c End of crucible
19 px 6.0
c Aluminum endcap
201 px 8.0
202 RCC 7 0 0 1 0 0 1.8
c Nickel foils
211 RPP 7 7.00256 -1.2 1.2 -0.95 0.95
212 RPP 9.196 9.19858 -1.05 1.05 5.85 7.75
c Gold Foils
221 RPP 9.196 9.201 -0.7 0.7 3.9 5.3
222 RPP 9.196 9.20104 -0.6 0.6 8.05 9.35
223 RPP 1.6 2.8 -11.00546 -11 -0.65 0.65
c Inside crucible and zinc cylinder
22 cx 0.95
c End of Surface Block followed by Blank Line
c +++
c Materials use photon library
c +++
c material 204 is air
m204 7014.62c -0.755636 8016.62c -0.231475 18040.80c -0.01288
c material 498 is titanium
m498 22048.80c -1 $MAT498

c material 486 is steel
m486 24050.62c -0.00793 $MAT486
24052.62c -0.159032 24053.62c -0.018378 24054.62c -0.004661
25055.62c -0.02 26054.62c -0.039605 26056.62c -0.638496
26057.62c -0.01488 26058.62c -0.002019 28058.62c -0.064024
28060.62c -0.025321 28061.62c -0.001115 28062.62c -0.003599
28064.62c -0.000942
c material 273 is zinc 68
m273 30064.80c -1 $MAT273
c material 283 is 6061 aluminum
m283 12024.80c 6.6898e-4 13027.62c 5.8593e-2 14028.62c 3.2037e-4
14029.62c 1.6222e-5 14030.62c 1.0768e-5 22048.80c 2.5469e-5
24050.62c 2.6495e-6 24052.62c 5.1093e-5 24053.62c 5.7929e-6
24054.62c 1.4421e-6 25055.62c 2.2197e-5 26054.62c 6.0121e-6
26056.62c 9.3463e-5 26057.62c 2.1399e-6 26058.62c 2.8532e-7
29063.62c 4.8671e-5 29065.62c 2.1695e-5
c material 284 is gold
m284 79197.70c -1
c material 285 is nickel
m285 28058.62c -0.6808 28060.62c -0.2622 28061.62c -0.01140
28062.62c -0.0364 28064.62c -0.0093
c m514 is water
m514 8016.62c -0.888106 1001 -0.111894
MX514:P j 0
c m272 is tungsten alloy 90% W, 3% Fe, 7% Ni
m272 74184.62c -.9 28058.62c -.07 26056.62c -.03
m320 6012.21c -1
c
c ************* Physics Data *******************************
c
mode n p e
mphys on
imp:n 0 1 19R

imp:p 0 1 19R
imp:e 0 1 19R
c Electron cutoff card
cut:e 1J .1
c Photon cutoff card
cut:p 1J .1
c
c Neutron cutoff card
cut:n 1J .1
c *************Electron physics card********************
phys:e 40.0 0 0 0 0 1 1 1 1 0 0 4J
c
c ***************Photon physics card***********
phys:p 40.0 0 0 1 0 J 0
c
c ***************Neutron physics card***********
phys:n 40.0 0 0 3J 0 -1 3J 0 0
c
c +++
c
c SOURCE DATA
c
c +++
c
c General source card
c cel=3 electrons start in beam pipe
c ERG=37.5 energy is 37.5 MeV
c DIR=1.0 all particles start in direction of VEC
c VEC=1 0 0 direction vector is along x-axis
c POS= -5, 0, 0
c RAD=D2 sample starting radius position on D2
c PAR=3 particle are electrons
c Distribution D2 information

```
c SI2 0.3 sampling radius is from 0 to 0.3
sdef erg=37.5 dir=1.0 vec=1 0 0 axs 1 0 0 pos= -1 0 0 rad=D2 par=3
SI2 0.3
c
c ***************************************************************************
c ******* Tallys ******************************************************
e0 0.1 20ilog 1 20ilog 40
c
c *** Photon tallies in foils ***
c
f104:p 151
fc104 Photon Tally in Au 1
c
f114:p 152
fc114 Photon Tally in Au 2
c
f124:p 153
fc124 Photon Tally in Au 3
c
f204:p 161
fc204 Photon Tally in Ni 1
c
f214:p 162
fc214 Photon Tally in Ni 2
c
c *** Neutron tallies in foils ***
c
f304:n 151
fc304 Neutron Tally in Au 1
c
f314:n 152
fc314 Neutron Tally in Au 2
c
```

```
f324:n 153
fc324 Neutron Tally in Au 3
c
f404:n 161
fc404 Neutron Tally in Ni 1
c
f414:n 162
fc414 Neutron Tally in Ni 2
c
nps 1e9
```

Figure A 1: MCNP script to determine flux distributions.

Table A 1: Detector efficiency from the IAC.

Source Cal	Source Act (Bq)	Energy Line	Branching Ratio	Total Counts	Error Counts	Count/live time	Error/live time	Source Current Activity (Bq)	Efficiency	Error Efficiency
7/1/2008 13:00	3.90E+05	80.989	0.342	43129	231	6.90E+02	3.70E+00	2.23E+05	9.07E-03	4.86E-05
7/1/2008 13:00	4.06E+05	121.78	0.2858	35132	199	7.53E+02	4.26E+00	2.62E+05	1.00E-02	5.69E-05
7/1/2008 13:00	4.06E+05	244.7	0.07583	6800	96	1.46E+02	2.06E+00	2.62E+05	7.33E-03	1.03E-04
7/1/2008 13:00	3.90E+05	276	0.0716	7323	96	1.17E+02	1.54E+00	2.23E+05	7.35E-03	9.64E-05
7/1/2008 13:00	3.90E+05	302.85	0.1833	17939	148	2.87E+02	2.37E+00	2.23E+05	7.04E-03	5.81E-05
7/1/2008 13:00	3.90E+05	355.999	0.622	53980	235	8.64E+02	3.76E+00	2.23E+05	6.24E-03	2.72E-05
7/15/2013 13:00	3.77E+05	511	1.807	31321	181	1.14E+03	6.58E+00	1.49E+05	4.24E-03	2.45E-05
7/1/2008 13:00	3.83E+05	661.66	0.8521	38298	198	1.05E+03	5.41E+00	3.14E+05	3.91E-03	2.02E-05
7/15/2013 13:00	3.77E+05	1274.577	0.9994	8311	93	3.02E+02	3.38E+00	1.49E+05	2.03E-03	2.27E-05
7/1/2008 13:00	4.06E+05	1085.87	0.1021	2314	77	4.96E+01	1.65E+00	2.62E+05	1.85E-03	6.16E-05
7/1/2008 13:00	3.86E+05	1173.237	0.99	10052	103	3.00E+02	3.07E+00	1.26E+05	2.41E-03	2.47E-05
7/1/2008 13:00	3.86E+05	1332.501	0.9998	9087	96	2.71E+02	2.86E+00	1.26E+05	2.16E-03	2.28E-05

Table A 2: MCNP photon flux for Ni1.

Energy (MeV)	**Differential Flux (1/(s*cm²*MeV))**	**Uncertainty (1/(s*cm²))**
0.105795	3.91635*10^13	2.58479*10^12
0.118055	4.16059*10^13	2.74599*10^12
0.131735	4.20594*10^13	2.77592*10^12
0.147	4.05875*10^13	2.67878*10^12
0.164035	3.90839*10^13	2.57954*10^12
0.183045	3.89957*10^13	2.57372*10^12
0.204255	3.68779*10^13	2.43394*10^12
0.227925	3.5187*10^13	2.32234*10^12
0.25434	3.40085*10^13	2.24456*10^12
0.283815	3.30906*10^13	2.18398*10^12
0.316705	3.19944*10^13	2.11163*10^12
0.353405	3.1136*10^13	2.05498*10^12
0.39436	3.04283*10^13	2.00827*10^12
0.44006	2.9581*10^13	1.95235*10^12
0.491055	5.80356*10^13	3.83035*10^12
0.54796	2.36428*10^13	1.56042*10^12
0.61146	2.20235*10^13	1.45355*10^12
0.68232	2.06059*10^13	1.35999*10^12
0.76139	1.92361*10^13	1.26959*10^12
0.84962	1.79917*10^13	1.18745*10^12
0.948075	1.67793*10^13	1.10743*10^12
1.096	1.52746*10^13	1.00812*10^12
1.30645	1.35215*10^13	8.9242*10^11
1.55735	1.1833*10^13	7.80975*10^11
1.85645	1.02408*10^13	6.75894*10^11
2.21295	8.75835*10^12	5.78051*10^11
2.6379	7.40135*10^12	4.88489*10^11
3.1445	6.18794*10^12	4.08404*10^11
3.74835	5.11287*10^12	3.37449*10^11
4.46815	4.17867*10^12	2.75792*10^11

5.3262	3.35562*10^12	2.21471*10^11
6.349	2.66672*10^12	1.76004*10^11
7.5682	2.09122*10^12	1.3802*10^11
9.02155	1.61603*10^12	1.06658*10^11
10.754	1.22757*10^12	8.10196*10^10
12.819	9.1544*10^11	6.04191*10^10
15.2805	6.7043*10^11	4.42484*10^10
18.215	4.83216*10^11	3.18923*10^10
21.713	3.38871*10^11	2.23655*10^10
25.8825	2.24806*10^11	1.48372*10^10
30.853	1.23416*10^11	8.14547*10^9
36.778	1.75217*10^10	1.15643*10^9

Table A 3: MCNP photon flux for Ni2.

Energy (MeV)	**Differential Flux (1/(s*cm²*MeV))**	**Uncertainty (1/(s*cm²))**
0.105795	2.53769*10^12	1.59874*10^11
0.118055	3.02879*10^12	1.90814*10^11
0.131735	3.33113*10^12	2.09861*10^11
0.147	3.47522*10^12	2.18939*10^11
0.164035	3.56282*10^12	2.24458*10^11
0.183045	3.73256*10^12	2.35151*10^11
0.204255	3.77476*10^12	2.3781*10^11
0.227925	3.84835*10^12	2.42446*10^11
0.25434	3.90528*10^12	2.46033*10^11
0.283815	3.92504*10^12	2.47278*10^11
0.316705	3.92204*10^12	2.47088*10^11
0.353405	3.89372*10^12	2.45304*10^11
0.39436	3.79516*10^12	2.39095*10^11
0.44006	3.64273*10^12	2.29492*10^11
0.491055	6.73216*10^12	4.24126*10^11
0.54796	2.69188*10^12	1.69588*10^11
0.61146	2.45998*10^12	1.54979*10^11
0.68232	2.21926*10^12	1.39814*10^11
0.76139	1.98215*10^12	1.24876*10^11
0.84962	1.74699*10^12	1.1006*10^11
0.948075	1.51968*10^12	9.57399*10^10
1.096	1.2522*10^12	7.88885*10^10
1.30645	9.75256*10^11	6.14411*10^10
1.55735	7.49717*10^11	4.72322*10^10
1.85645	5.74868*10^11	3.62167*10^10
2.21295	4.39831*10^11	2.77093*10^10
2.6379	3.40539*10^11	2.1454*10^10
3.1445	2.6187*10^11	1.64978*10^10
3.74835	2.01946*10^11	1.27226*10^10
4.46815	1.54335*10^11	9.7231*10^9

5.3262	1.16589*10^11	7.34512*10^9
6.349	8.76027*10^10	5.51897*10^9
7.5682	6.42153*10^10	4.04556*10^9
9.02155	4.63028*10^10	2.91707*10^9
10.754	3.25334*10^10	2.0496*10^9
12.819	2.19347*10^10	1.38189*10^9
15.2805	1.41094*10^10	8.8889*10^8
18.215	8.39885*10^9	5.29127*10^8
21.713	4.37934*10^9	2.75899*10^8
25.8825	1.7728*10^9	1.11686*10^8
30.853	3.85887*10^8	2.43109*10^7
36.778	1.03592*10^7	652633

Table A 4: Normalized photon flux for Ni1.

Energy (MeV)	**Differential Flux (1/(s*cm²*MeV))**	**Uncertainty (1/(s*cm²))**
0.105795	2.94684*10^13	2.29854*10^12
0.118055	3.13062*10^13	2.44189*10^12
0.131735	3.16475*10^13	2.4685*10^12
0.147	3.05399*10^13	2.38211*10^12
0.164035	2.94085*10^13	2.29386*10^12
0.183045	2.93422*10^13	2.28869*10^12
0.204255	2.77486*10^13	2.16439*10^12
0.227925	2.64763*10^13	2.06515*10^12
0.25434	2.55896*10^13	1.99599*10^12
0.283815	2.48989*10^13	1.94212*10^12
0.316705	2.40741*10^13	1.87778*10^12
0.353405	2.34282*10^13	1.8274*10^12
0.39436	2.28956*10^13	1.78586*10^12
0.44006	2.22581*10^13	1.73613*10^12
0.491055	4.36687*10^13	3.40616*10^12
0.54796	1.77899*10^13	1.38761*10^12
0.61146	1.65715*10^13	1.29258*10^12
0.68232	1.55048*10^13	1.20937*10^12
0.76139	1.44742*10^13	1.12898*10^12
0.84962	1.35378*10^13	1.05595*10^12
0.948075	1.26255*10^13	9.84791*10^11
1.096	1.14933*10^13	8.96476*10^11
1.30645	1.01742*10^13	7.93589*10^11
1.55735	8.90366*10^12	6.94485*10^11
1.85645	7.70567*10^12	6.01042*10^11
2.21295	6.59019*10^12	5.14035*10^11
2.6379	5.56912*10^12	4.34391*10^11
3.1445	4.65609*10^12	3.63175*10^11
3.74835	3.84716*10^12	3.00078*10^11
4.46815	3.14422*10^12	2.45249*10^11

5.3262	2.52493*10^12	1.96944*10^11
6.349	2.00656*10^12	1.56512*10^11
7.5682	1.57353*10^12	1.22735*10^11
9.02155	1.21597*10^12	9.4846*10^10
10.754	9.2368*10^11	7.2047*10^10
12.819	6.88819*10^11	5.37279*10^10
15.2805	5.04463*10^11	3.93481*10^10
18.215	3.63594*10^11	2.83603*10^10
21.713	2.54982*10^11	1.98886*10^10
25.8825	1.69154*10^11	1.3194*10^10
30.853	9.28641*10^10	7.2434*10^9
36.778	1.31841*10^10	1.02836*10^9

Table A 5: Normalized photon flux for Ni2.

Energy (MeV)	**Differential Flux (1/(s*cm²*MeV))**	**Uncertainty (1/(s*cm²))**
0.105795	1.90948*10^12	1.4512*10^11
0.118055	2.279*10^12	1.73204*10^11
0.131735	2.5065*10^12	1.90494*10^11
0.147	2.61492*10^12	1.98734*10^11
0.164035	2.68083*10^12	2.03743*10^11
0.183045	2.80855*10^12	2.1345*10^11
0.204255	2.84031*10^12	2.15863*10^11
0.227925	2.89568*10^12	2.20071*10^11
0.25434	2.93851*10^12	2.23327*10^11
0.283815	2.95338*10^12	2.24457*10^11
0.316705	2.95112*10^12	2.24285*10^11
0.353405	2.92981*10^12	2.22666*10^11
0.39436	2.85565*10^12	2.1703*10^11
0.44006	2.74096*10^12	2.08313*10^11
0.491055	5.06559*10^12	3.84985*10^11
0.54796	2.02549*10^12	1.53938*10^11
0.61146	1.851*10^12	1.40676*10^11
0.68232	1.66988*10^12	1.26911*10^11
0.76139	1.49146*10^12	1.13351*10^11
0.84962	1.31451*10^12	9.9903*10^10
0.948075	1.14348*10^12	8.69043*10^10
1.096	9.42211*10^11	7.16081*10^10
1.30645	7.33827*10^11	5.57709*10^10
1.55735	5.64122*10^11	4.28733*10^10
1.85645	4.32557*10^11	3.28743*10^10
2.21295	3.30949*10^11	2.51521*10^10
2.6379	2.56237*10^11	1.9474*10^10
3.1445	1.97043*10^11	1.49753*10^10
3.74835	1.51954*10^11	1.15485*10^10
4.46815	1.16129*10^11	8.82578*10^9

5.3262	8.77271*10^10	6.66726*10^9
6.349	6.59163*10^10	5.00964*10^9
7.5682	4.83186*10^10	3.67221*10^9
9.02155	3.48403*10^10	2.64787*10^9
10.754	2.44796*10^10	1.86045*10^9
12.819	1.65047*10^10	1.25435*10^9
15.2805	1.06165*10^10	8.06857*10^8
18.215	6.31968*10^9	4.80296*10^8
21.713	3.29522*10^9	2.50437*10^8
25.8825	1.33394*10^9	1.01379*10^8
30.853	2.90359*10^8	2.20673*10^7
36.778	7.79478*10^6	592403

Table A 6: MCNP photon flux for Au1.

Energy (MeV)	**Differential Flux (1/(s*cm²*MeV))**	**Uncertainty (1/(s*cm²))**
0.105795	3.12818*10^12	4.69227*10^11
0.118055	3.82235*10^12	5.73352*10^11
0.131735	4.31389*10^12	6.47084*10^11
0.147	4.57946*10^12	6.86919*10^11
0.164035	4.78182*10^12	7.17272*10^11
0.183045	5.13104*10^12	7.69656*10^11
0.204255	5.27026*10^12	7.90539*10^11
0.227925	5.49148*10^12	8.23722*10^11
0.25434	5.64675*10^12	8.47013*10^11
0.283815	5.8103*10^12	8.71545*10^11
0.316705	5.88337*10^12	8.82506*10^11
0.353405	5.9103*10^12	8.86546*10^11
0.39436	5.81231*10^12	8.71847*10^11
0.44006	5.67568*10^12	8.51353*10^11
0.491055	9.9883*10^12	1.49824*10^12
0.54796	4.40948*10^12	6.61422*10^11
0.61146	4.07698*10^12	6.11547*10^11
0.68232	3.75962*10^12	5.63942*10^11
0.76139	3.42529*10^12	5.13793*10^11
0.84962	3.10136*10^12	4.65203*10^11
0.948075	2.77657*10^12	4.16486*10^11
1.096	2.39815*10^12	3.59722*10^11
1.30645	1.96906*10^12	2.95359*10^11
1.55735	1.58467*10^12	2.377*10^11
1.85645	1.26452*10^12	1.89678*10^11
2.21295	9.96843*10^11	1.49527*10^11
2.6379	7.80297*10^11	1.17045*10^11
3.1445	6.08481*10^11	9.12721*10^10
3.74835	4.7317*10^11	7.09755*10^10
4.46815	3.6645*10^11	5.49675*10^10

5.3262	2.81407*10^11	4.22111*10^10
6.349	2.14157*10^11	3.21236*10^10
7.5682	1.61423*10^11	2.42134*10^10
9.02155	1.1967*10^11	1.79505*10^10
10.754	8.69326*10^10	1.30399*10^10
12.819	6.11805*10^10	9.17707*10^9
15.2805	4.17156*10^10	6.25734*10^9
18.215	2.68386*10^10	4.02579*10^9
21.713	1.55777*10^10	2.33665*10^9
25.8825	7.41405*10^9	1.11211*10^9
30.853	2.03032*10^9	3.04548*10^8
36.778	6.30215*10^7	9.45323*10^6

Table A 7: MCNP photon flux for Au2.

Energy (MeV)	**Differential Flux (1/(s*cm²*MeV))**	**Uncertainty (1/(s*cm²))**
0.105795	1.23466*10^12	1.97546*10^11
0.118055	1.64406*10^12	2.6305*10^11
0.131735	1.96649*10^12	3.14639*10^11
0.147	2.20815*10^12	3.53303*10^11
0.164035	2.38175*10^12	3.81081*10^11
0.183045	2.58384*10^12	4.13414*10^11
0.204255	2.67331*10^12	4.2773*10^11
0.227925	2.75531*10^12	4.40849*10^11
0.25434	2.81935*10^12	4.51097*10^11
0.283815	2.84737*10^12	4.55579*10^11
0.316705	2.8565*10^12	4.5704*10^11
0.353405	2.81304*10^12	4.50086*10^11
0.39436	2.71633*10^12	4.34613*10^11
0.44006	2.6035*10^12	4.1656*10^11
0.491055	4.95911*10^12	7.93457*10^11
0.54796	1.88444*10^12	3.01511*10^11
0.61146	1.70095*10^12	2.72153*10^11
0.68232	1.50198*10^12	2.40318*10^11
0.76139	1.31623*10^12	2.10597*10^11
0.84962	1.13138*10^12	1.81021*10^11
0.948075	9.62345*10^11	1.53975*10^11
1.096	7.69455*10^11	1.23113*10^11
1.30645	5.78066*10^11	9.24906*10^10
1.55735	4.3644*10^11	6.98305*10^10
1.85645	3.28487*10^11	5.25579*10^10
2.21295	2.52593*10^11	4.04149*10^10
2.6379	1.93553*10^11	3.09685*10^10
3.1445	1.48257*10^11	2.37211*10^10
3.74835	1.13045*10^11	1.80871*10^10
4.46815	8.6507*10^10	1.38411*10^10

5.3262	6.37235*10^10	1.01958*10^10
6.349	4.72955*10^10	7.56728*10^9
7.5682	3.43027*10^10	5.48842*10^9
9.02155	2.43454*10^10	3.89527*10^9
10.754	1.65238*10^10	2.64381*10^9
12.819	1.08178*10^10	1.73085*10^9
15.2805	6.72388*10^9	1.07582*10^9
18.215	3.81681*10^9	6.1069*10^8
21.713	1.87797*10^9	3.00475*10^8
25.8825	6.82339*10^8	1.09174*10^8
30.853	1.3665*10^8	2.18639*10^7
36.778	3.72496*10^6	595994

Table A 8: MCNP photon flux for Au3.

Energy (MeV)	**Differential Flux (1/(s*cm²*MeV))**	**Uncertainty (1/(s*cm²))**
0.105795	1.21785*10^12	3.53176*10^11
0.118055	1.62385*10^12	4.70917*10^11
0.131735	1.99705*10^12	5.79144*10^11
0.147	2.29039*10^12	6.64212*10^11
0.164035	2.52812*10^12	7.33155*10^11
0.183045	2.71091*10^12	7.86163*10^11
0.204255	2.71235*10^12	7.86583*10^11
0.227925	2.65308*10^12	7.69392*10^11
0.25434	2.56704*10^12	7.44443*10^11
0.283815	2.42283*10^12	7.0262*10^11
0.316705	2.22937*10^12	6.46518*10^11
0.353405	2.03726*10^12	5.90805*10^11
0.39436	1.77951*10^12	5.16059*10^11
0.44006	1.51576*10^12	4.3957*10^11
0.491055	3.57625*10^12	1.03711*10^12
0.54796	7.20688*10^11	2.08999*10^11
0.61146	5.61774*10^11	1.62915*10^11
0.68232	4.48641*10^11	1.30106*10^11
0.76139	3.66049*10^11	1.06154*10^11
0.84962	3.03668*10^11	8.80637*10^10
0.948075	2.55012*10^11	7.39535*10^10
1.096	2.02834*10^11	5.88219*10^10
1.30645	1.54876*10^11	4.4914*10^10
1.55735	1.18657*10^11	3.44104*10^10
1.85645	9.01746*10^10	2.61506*10^10
2.21295	6.79741*10^10	1.97125*10^10
2.6379	5.05349*10^10	1.46551*10^10
3.1445	3.73695*10^10	1.08371*10^10
3.74835	2.69947*10^10	7.82847*10^9
4.46815	1.94585*10^10	5.64297*10^9

5.3262	1.35468*10^10	3.92858*10^9
6.349	9.21715*10^9	2.67297*10^9
7.5682	6.21548*10^9	1.80249*10^9
9.02155	3.94949*10^9	1.14535*10^9
10.754	2.31499*10^9	6.71348*10^8
12.819	1.35331*10^9	3.9246*10^8
15.2805	7.21102*10^8	2.09119*10^8
18.215	3.53973*10^8	1.02652*10^8
21.713	1.57222*10^8	4.55943*10^7
25.8825	5.33951*10^7	1.54846*10^7
30.853	1.62016*10^7	4.69846*10^6
36.778	275103	79779.9

Table A 9: Normalized photon flux for Au1.

Energy (MeV)	**Differential Flux (1/(s*cm²*MeV))**	**Uncertainty (1/(s*cm²))**
0.105795	2.35379*10^12	3.76606*10^11
0.118055	2.87611*10^12	4.60178*10^11
0.131735	3.24597*10^12	5.19355*10^11
0.147	3.4458*10^12	5.51327*10^11
0.164035	3.59806*10^12	5.75689*10^11
0.183045	3.86083*10^12	6.17733*10^11
0.204255	3.96558*10^12	6.34494*10^11
0.227925	4.13204*10^12	6.61127*10^11
0.25434	4.24888*10^12	6.79821*10^11
0.283815	4.37194*10^12	6.9951*10^11
0.316705	4.42692*10^12	7.08307*10^11
0.353405	4.44719*10^12	7.1155*10^11
0.39436	4.37345*10^12	6.99752*10^11
0.44006	4.27065*10^12	6.83303*10^11
0.491055	7.51565*10^12	1.2025*10^12
0.54796	3.3179*10^12	5.30864*10^11
0.61146	3.06771*10^12	4.90833*10^11
0.68232	2.82891*10^12	4.52625*10^11
0.76139	2.57734*10^12	4.12375*10^11
0.84962	2.3336*10^12	3.73377*10^11
0.948075	2.08922*10^12	3.34275*10^11
1.096	1.80448*10^12	2.88716*10^11
1.30645	1.48161*10^12	2.37058*10^11
1.55735	1.19238*10^12	1.90781*10^11
1.85645	9.51485*10^11	1.52238*10^11
2.21295	7.50071*10^11	1.20011*10^11
2.6379	5.87132*10^11	9.39411*10^10
3.1445	4.57849*10^11	7.32558*10^10
3.74835	3.56035*10^11	5.69656*10^10
4.46815	2.75734*10^11	4.41174*10^10

5.3262	2.11744*10^11	3.3879*10^10
6.349	1.61142*10^11	2.57827*10^10
7.5682	1.21462*10^11	1.94339*10^10
9.02155	9.00454*10^10	1.44073*10^10
10.754	6.54121*10^10	1.04659*10^10
12.819	4.6035*10^10	7.3656*10^9
15.2805	3.13887*10^10	5.0222*10^9
18.215	2.01946*10^10	3.23114*10^9
21.713	1.17213*10^10	1.87542*10^9
25.8825	5.57867*10^9	8.92587*10^8
30.853	1.52771*10^9	2.44433*10^8
36.778	4.74203*10^7	7.58725*10^6

Table A 10: Normalized photon flux for Au2.

Energy (MeV)	**Differential Flux (1/(s*cm²*MeV))**	**Uncertainty (1/(s*cm²))**
0.105795	9.29016*10^11	1.48642*10^11
0.118055	1.23707*10^12	1.97931*10^11
0.131735	1.47968*10^12	2.36749*10^11
0.147	1.66151*10^12	2.65842*10^11
0.164035	1.79214*10^12	2.86743*10^11
0.183045	1.9442*10^12	3.11072*10^11
0.204255	2.01152*10^12	3.21844*10^11
0.227925	2.07322*10^12	3.31715*10^11
0.25434	2.12141*10^12	3.39426*10^11
0.283815	2.14249*10^12	3.42799*10^11
0.316705	2.14936*10^12	3.43898*10^11
0.353405	2.11666*10^12	3.38665*10^11
0.39436	2.04389*10^12	3.27023*10^11
0.44006	1.959*10^12	3.13439*10^11
0.491055	3.73146*10^12	5.97034*10^11
0.54796	1.41794*10^12	2.26871*10^11
0.61146	1.27988*10^12	2.0478*10^11
0.68232	1.13016*10^12	1.80826*10^11
0.76139	9.90392*10^11	1.58463*10^11
0.84962	8.51304*10^11	1.36209*10^11
0.948075	7.24112*10^11	1.15858*10^11
1.096	5.78973*10^11	9.26357*10^10
1.30645	4.34964*10^11	6.95942*10^10
1.55735	3.28398*10^11	5.25437*10^10
1.85645	2.47169*10^11	3.9547*10^10
2.21295	1.90063*10^11	3.041*10^10
2.6379	1.45638*10^11	2.33021*10^10
3.1445	1.11555*10^11	1.78488*10^10
3.74835	8.50599*10^10	1.36096*10^10
4.46815	6.50919*10^10	1.04147*10^10

5.3262	4.79485*10^10	7.67176*10^9
6.349	3.55873*10^10	5.69397*10^9
7.5682	2.58109*10^10	4.12974*10^9
9.02155	1.83186*10^10	2.93098*10^9
10.754	1.24333*10^10	1.98933*10^9
12.819	8.13981*10^9	1.30237*10^9
15.2805	5.05936*10^9	8.09498*10^8
18.215	2.87195*10^9	4.59511*10^8
21.713	1.41307*10^9	2.26091*10^8
25.8825	5.13423*10^8	8.21477*10^7
30.853	1.02822*10^8	1.64514*10^7
36.778	2.80283*10^6	448453

Table A 11: Normalized photon flux for Au3.

Energy (MeV)	**Differential Flux (1/(s*cm²*MeV))**	**Uncertainty (1/(s*cm²))**
0.105795	9.16366*10^11	2.65746*10^11
0.118055	1.22186*10^12	3.54339*10^11
0.131735	1.50267*10^12	4.35775*10^11
0.147	1.72339*10^12	4.99784*10^11
0.164035	1.90227*10^12	5.51659*10^11
0.183045	2.03981*10^12	5.91546*10^11
0.204255	2.0409*10^12	5.91861*10^11
0.227925	1.9963*10^12	5.78926*10^11
0.25434	1.93156*10^12	5.60153*10^11
0.283815	1.82305*10^12	5.28684*10^11
0.316705	1.67748*10^12	4.8647*10^11
0.353405	1.53293*10^12	4.44549*10^11
0.39436	1.33899*10^12	3.88306*10^11
0.44006	1.14053*10^12	3.30753*10^11
0.491055	2.69093*10^12	7.80371*10^11
0.54796	5.42279*10^11	1.57261*10^11
0.61146	4.22705*10^11	1.22584*10^11
0.68232	3.37579*10^11	9.78978*10^10
0.76139	2.75432*10^11	7.98753*10^10
0.84962	2.28494*10^11	6.62632*10^10
0.948075	1.91883*10^11	5.5646*10^10
1.096	1.52622*10^11	4.42603*10^10
1.30645	1.16536*10^11	3.37954*10^10
1.55735	8.92827*10^10	2.5892*10^10
1.85645	6.78515*10^10	1.96769*10^10
2.21295	5.11469*10^10	1.48326*10^10
2.6379	3.80248*10^10	1.10272*10^10
3.1445	2.81185*10^10	8.15437*10^9
3.74835	2.03121*10^10	5.8905*10^9
4.46815	1.46415*10^10	4.24603*10^9

5.3262	1.01933*10^10	2.95604*10^9
6.349	6.93541*10^9	2.01127*10^9
7.5682	4.67681*10^9	1.35628*10^9
9.02155	2.97177*10^9	8.61815*10^8
10.754	1.74191*10^9	5.05153*10^8
12.819	1.01829*10^9	2.95305*10^8
15.2805	5.4259*10^8	1.57351*10^8
18.215	2.66346*10^8	7.72402*10^7
21.713	1.18301*10^8	3.43073*10^7
25.8825	4.0177*10^7	1.16513*10^7
30.853	1.21908*10^7	3.53534*10^6
36.778	207000	60030.1

Table A 12: MCNP neutron flux for Ni1.

Energy (MeV)	**Differential Flux (1/(s*cm^2*MeV))**	**Uncertainty (1/(s*cm^2))**
0.105795	5.20554*10^9	1.19727*10^9
0.118055	5.13824*10^9	1.1818*10^9
0.131735	6.88158*10^9	1.58276*10^9
0.147	3.85333*10^9	8.86265*10^8
0.164035	3.59605*10^9	8.27092*10^8
0.183045	4.14259*10^9	9.52796*10^8
0.204255	3.76707*10^9	8.66425*10^8
0.227925	4.5191*10^9	1.03939*10^9
0.25434	4.04846*10^9	9.31145*10^8
0.283815	3.9319*10^9	9.04337*10^8
0.316705	3.55987*10^9	8.18771*10^8
0.353405	3.94077*10^9	9.06377*10^8
0.39436	3.97673*10^9	9.14649*10^8
0.44006	3.18695*10^9	7.32999*10^8
0.491055	3.50555*10^9	8.06276*10^8
0.54796	3.35481*10^9	7.71607*10^8
0.61146	3.43837*10^9	7.90826*10^8
0.68232	3.67516*10^9	8.45286*10^8
0.76139	3.48358*10^9	8.01223*10^8
0.84962	3.27376*10^9	7.52965*10^8
0.948075	3.01742*10^9	6.94007*10^8
1.096	2.8521*10^9	6.55982*10^8
1.30645	2.60634*10^9	5.99459*10^8
1.55735	2.31496*10^9	5.32441*10^8
1.85645	1.95529*10^9	4.49718*10^8
2.21295	1.5993*10^9	3.67839*10^8
2.6379	1.3337*10^9	3.0675*10^8
3.1445	1.02391*10^9	2.35499*10^8
3.74835	7.97011*10^8	1.83312*10^8
4.46815	6.06228*10^8	1.39433*10^8

5.3262	3.98395*10^8	9.16309*10^7
6.349	2.63936*10^8	6.07053*10^7
7.5682	1.53892*10^8	3.53951*10^7
9.02155	8.81343*10^7	2.02709*10^7
10.754	3.89184*10^7	8.95122*10^6
12.819	1.75661*10^7	4.04021*10^6
15.2805	5.71271*10^6	1.31392*10^6
18.215	1.21106*10^6	278543
21.713	178697	41100.4
25.8825	0	0
30.853	0	0
36.778	0	0

Table A 13: MCNP neutron flux for Ni2.

Energy (MeV)	**Differential Flux (1/(s*cm²*MeV))**	**Uncertainty (1/(s*cm²))**
0.105795	8.00791*10^8	2.72269*10^8
0.118055	9.27122*10^8	3.15221*10^8
0.131735	7.73627*10^8	2.63033*10^8
0.147	6.54878*10^8	2.22658*10^8
0.164035	6.53841*10^8	2.22306*10^8
0.183045	7.52483*10^8	2.55844*10^8
0.204255	7.28185*10^8	2.47583*10^8
0.227925	5.98157*10^8	2.03373*10^8
0.25434	6.20995*10^8	2.11138*10^8
0.283815	6.05152*10^8	2.05752*10^8
0.316705	5.80398*10^8	1.97335*10^8
0.353405	6.10454*10^8	2.07554*10^8
0.39436	6.00603*10^8	2.04205*10^8
0.44006	4.56422*10^8	1.55183*10^8
0.491055	5.56265*10^8	1.8913*10^8
0.54796	5.80902*10^8	1.97507*10^8
0.61146	5.37021*10^8	1.82587*10^8
0.68232	5.78722*10^8	1.96766*10^8
0.76139	5.15879*10^8	1.75399*10^8
0.84962	5.14529*10^8	1.7494*10^8
0.948075	4.04891*10^8	1.37663*10^8
1.096	4.3729*10^8	1.48679*10^8
1.30645	3.74419*10^8	1.27302*10^8
1.55735	3.27841*10^8	1.11466*10^8
1.85645	2.67662*10^8	9.10051*10^7
2.21295	2.1288*10^8	7.23791*10^7
2.6379	1.71558*10^8	5.83298*10^7
3.1445	1.23878*10^8	4.21186*10^7
3.74835	8.18143*10^7	2.78169*10^7
4.46815	5.96289*10^7	2.02738*10^7

5.3262	3.94992*10^7	1.34297*10^7
6.349	2.80484*10^7	9.53645*10^6
7.5682	1.39307*10^7	4.73644*10^6
9.02155	7.64098*10^6	2.59793*10^6
10.754	4.9205*10^6	1.67297*10^6
12.819	1.53321*10^6	521290
15.2805	1.11755*10^6	379966
18.215	41594.5	14142.1
21.713	31539.2	10723.3
25.8825	0	0
30.853	0	0
36.778	0	0

Table A 14: Normalized neutron flux for Ni1.

Energy (MeV)	**Differential Flux (1/(s*cm²*MeV))**	**Uncertainty (1/(s*cm²))**
0.105795	6.70714*10^9	1.54264*10^9
0.118055	6.62043*10^9	1.5227*10^9
0.131735	8.86665*10^9	2.03933*10^9
0.147	4.96486*10^9	1.14192*10^9
0.164035	4.63337*10^9	1.06568*10^9
0.183045	5.33757*10^9	1.22764*10^9
0.204255	4.85372*10^9	1.11636*10^9
0.227925	5.82269*10^9	1.33922*10^9
0.25434	5.21628*10^9	1.19974*10^9
0.283815	5.0661*10^9	1.1652*10^9
0.316705	4.58676*10^9	1.05495*10^9
0.353405	5.07753*10^9	1.16783*10^9
0.39436	5.12387*10^9	1.17849*10^9
0.44006	4.10627*10^9	9.44442*10^8
0.491055	4.51676*10^9	1.03886*10^9
0.54796	4.32255*10^9	9.94186*10^8
0.61146	4.43021*10^9	1.01895*10^9
0.68232	4.7353*10^9	1.08912*10^9
0.76139	4.48846*10^9	1.03235*10^9
0.84962	4.21812*10^9	9.70167*10^8
0.948075	3.88783*10^9	8.94201*10^8
1.096	3.67482*10^9	8.45208*10^8
1.30645	3.35817*10^9	7.72379*10^8
1.55735	2.98274*10^9	6.86029*10^8
1.85645	2.51932*10^9	5.79444*10^8
2.21295	2.06064*10^9	4.73947*10^8
2.6379	1.71842*10^9	3.95236*10^8
3.1445	1.31927*10^9	3.03431*10^8
3.74835	1.02692*10^9	2.36191*10^8
4.46815	7.81102*10^8	1.79653*10^8

5.3262	5.13317*10^8	1.18063*10^8
6.349	3.40071*10^8	7.82164*10^7
7.5682	1.98284*10^8	4.56053*10^7
9.02155	1.13558*10^8	2.61183*10^7
10.754	5.01448*10^7	1.15333*10^7
12.819	2.26333*10^7	5.20566*10^6
15.2805	7.3606*10^6	1.69294*10^6
18.215	1.5604*10^6	358892
21.713	230245	52956.3
25.8825	0	0
30.853	0	0
36.778	0	0

Table A 15: Normalized neutron flux for Ni2.

Energy (MeV)	**Differential Flux (1/(s*cm²*MeV))**	**Uncertainty (1/(s*cm²))**
0.105795	1.03179*10^9	4.02398*10^8
0.118055	1.19456*10^9	4.65879*10^8
0.131735	9.96789*10^8	3.88748*10^8
0.147	8.43785*10^8	3.29076*10^8
0.164035	8.42449*10^8	3.28555*10^8
0.183045	9.69545*10^8	3.78123*10^8
0.204255	9.38239*10^8	3.65913*10^8
0.227925	7.70702*10^8	3.00574*10^8
0.25434	8.00129*10^8	3.1205*10^8
0.283815	7.79715*10^8	3.04089*10^8
0.316705	7.47821*10^8	2.9165*10^8
0.353405	7.86546*10^8	3.06753*10^8
0.39436	7.73854*10^8	3.01803*10^8
0.44006	5.88082*10^8	2.29352*10^8
0.491055	7.16726*10^8	2.79523*10^8
0.54796	7.48469*10^8	2.91903*10^8
0.61146	6.91931*10^8	2.69853*10^8
0.68232	7.45661*10^8	2.90808*10^8
0.76139	6.64691*10^8	2.59229*10^8
0.84962	6.62951*10^8	2.58551*10^8
0.948075	5.21687*10^8	2.03458*10^8
1.096	5.63431*10^8	2.19738*10^8
1.30645	4.82424*10^8	1.88145*10^8
1.55735	4.22411*10^8	1.6474*10^8
1.85645	3.44872*10^8	1.345*10^8
2.21295	2.74287*10^8	1.06972*10^8
2.6379	2.21046*10^8	8.6208*10^7
3.1445	1.59612*10^8	6.22488*10^7
3.74835	1.05415*10^8	4.11117*10^7
4.46815	7.68295*10^7	2.99635*10^7

5.3262	5.08932*10^7	1.98484*10^7
6.349	3.61393*10^7	1.40943*10^7
7.5682	1.79492*10^7	7.00019*10^6
9.02155	9.84511*10^6	3.83959*10^6
10.754	6.33987*10^6	2.47255*10^6
12.819	1.97548*10^6	770436
15.2805	1.43992*10^6	561567
18.215	53592.9	20901.2
21.713	40637.1	15848.5
25.8825	0	0
30.853	0	0
36.778	0	0

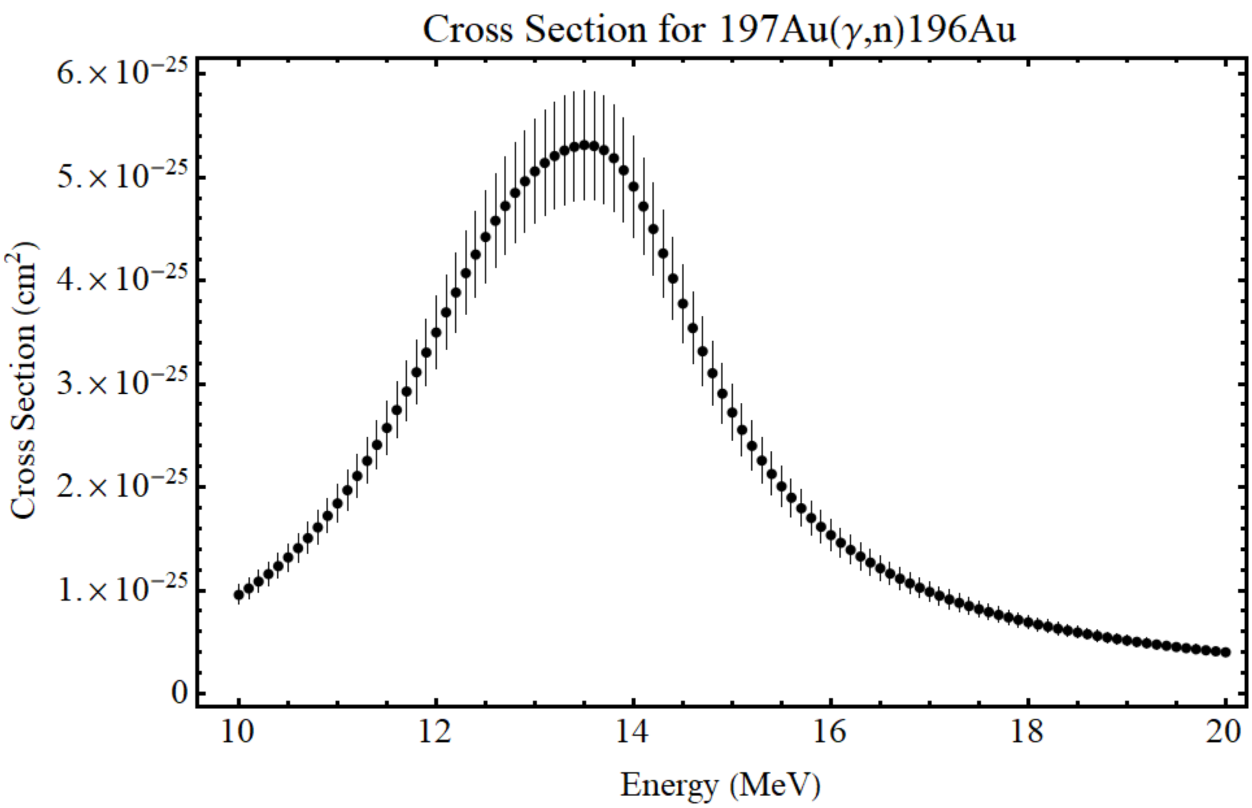

Figure A 2: Cross section for 197Au(γ,n)196Au [2].

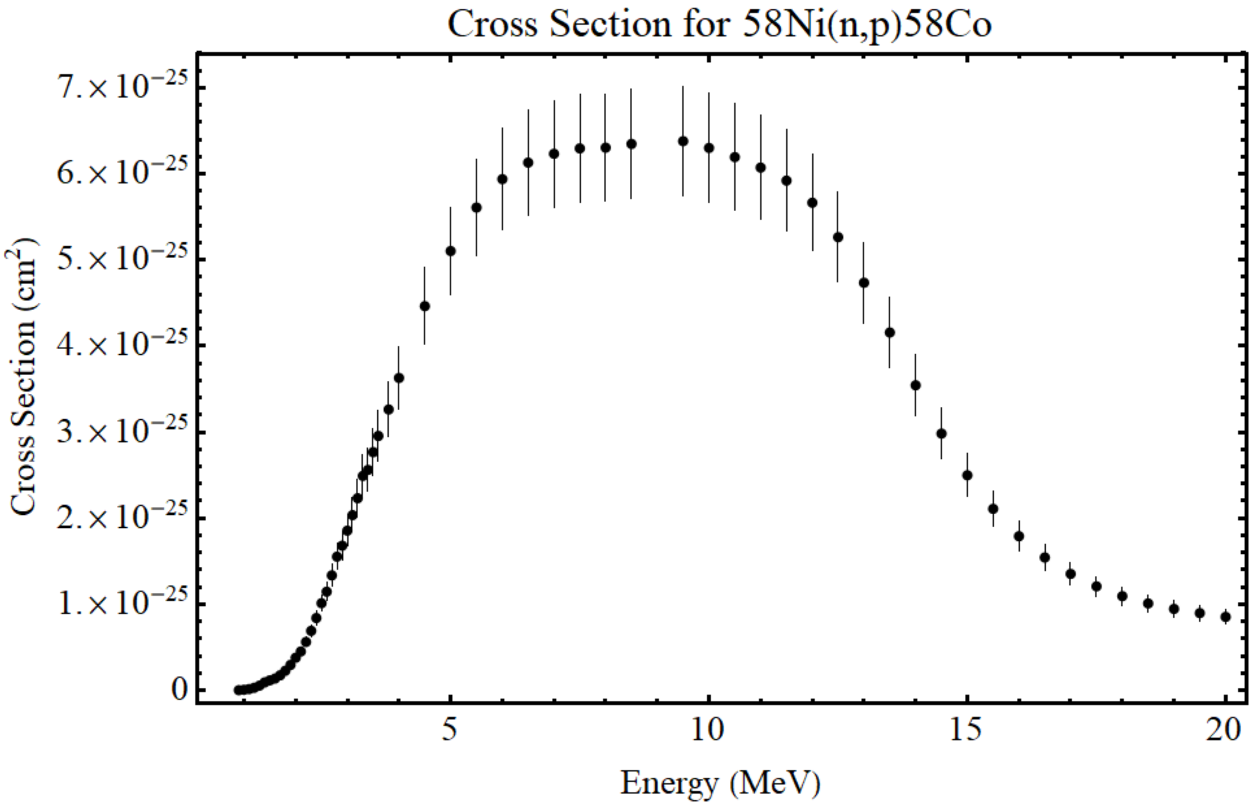

Figure A 3: Cross section for 58Ni(n,p)58Co [4].

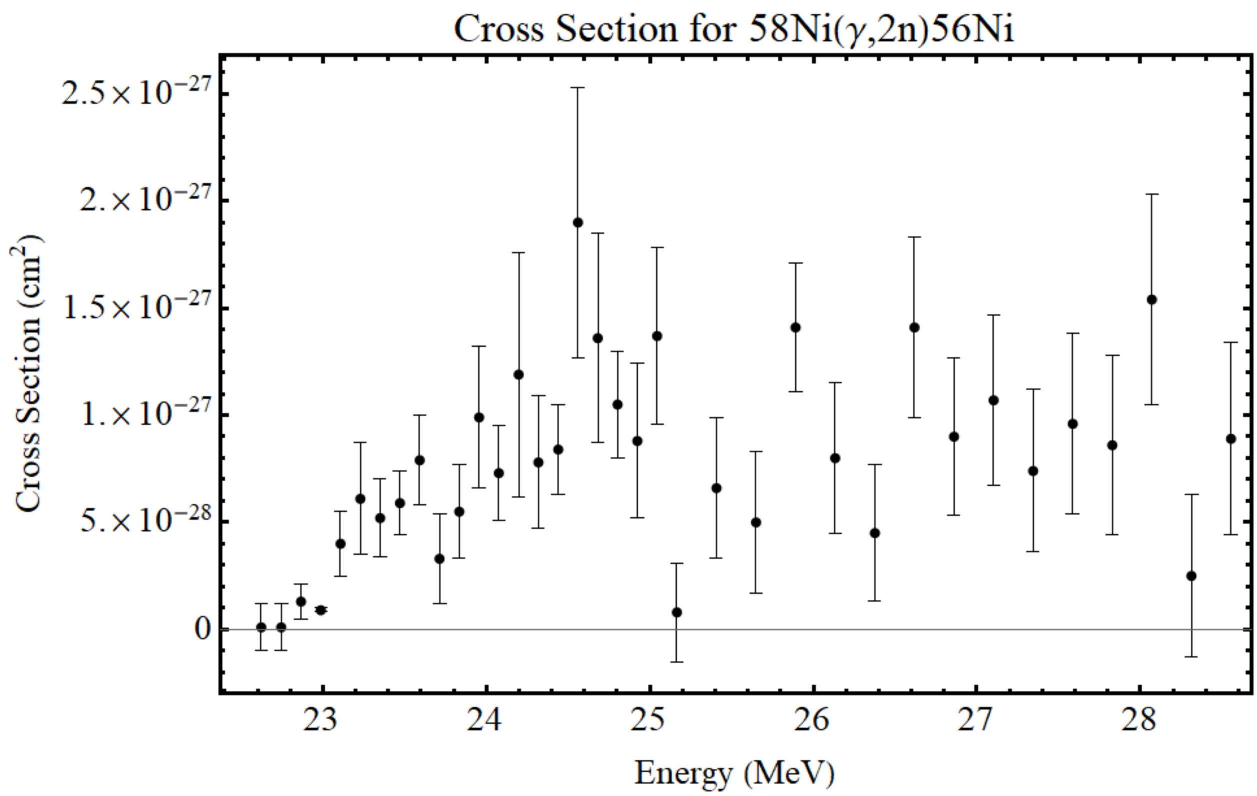

Figure A 4: Cross section for 58Ni(γ,2n)56Ni [3].

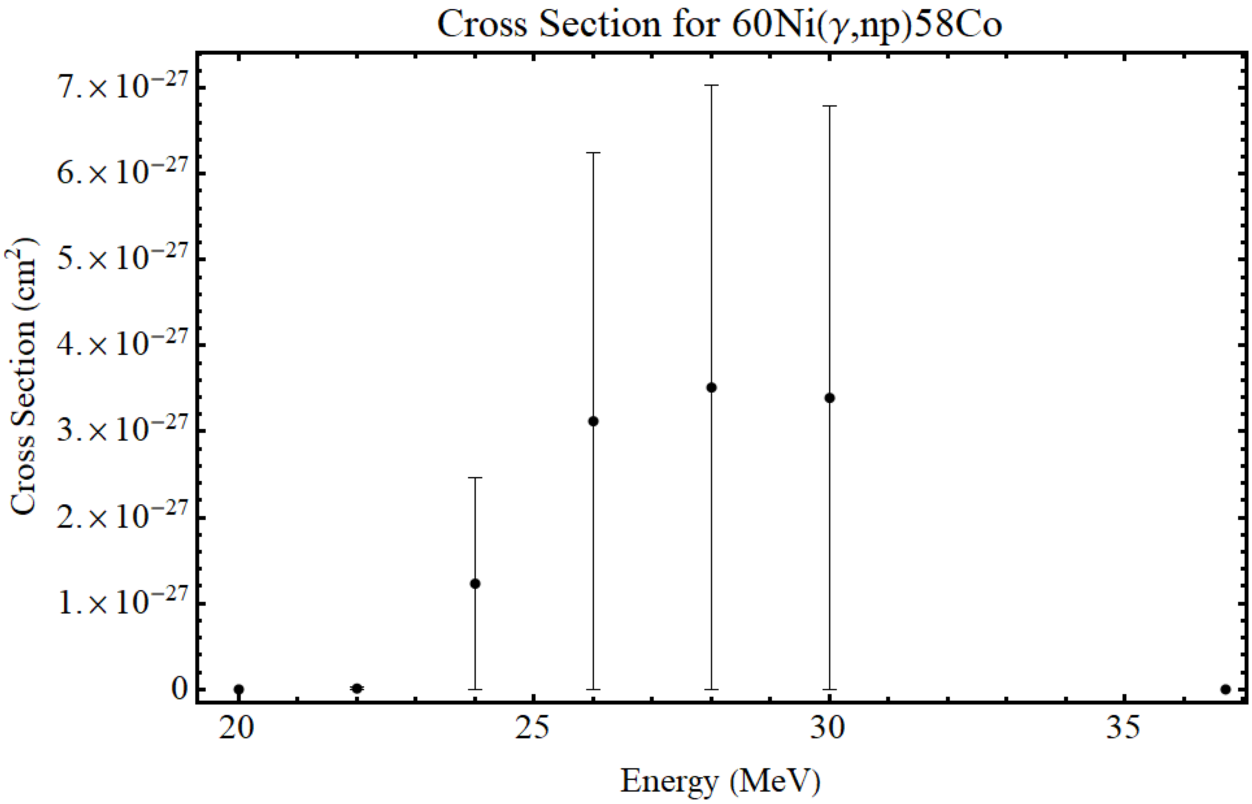

Figure A 5: Cross section for 60Ni(γ,np)58Co [5] .